Eclética Química Journal

Original review
iq.unesp.br/ecletica

| Vol. 44 | n. 1 | 2019 |

A review on the state-of-the-art advances for CO_2 electro-chemical reduction using metal complex molecular catalysts

Hitler Louis[1, 2+], Ozioma Udochukwu Akakuru[2, 3], Philip Monday[1], Oyebanji Oluwatomisin Funmilayo[4]

[1] University of Chinese Academy of Sciences, National Centre for Nanoscience and Technology, CAS Centre for Excellence in Nanoscience, CAS Key Laboratory for Nanosystem and Hierarchical Fabrication, Beijing, China.
[2] University of Calabar, Faculty of Physical Sciences, Department of Pure and Applied Chemistry, Calabar, Cross River State, Nigeria
[3] University of Chinese Academy of Sciences, Ningbo Institute of Materials Technology and Engineering, Zhejiang, P.R. China
[4] University of Ibadan, Faculty of Physical Sciences, Department of Chemistry, Ibadan, Nigeria

[+] Corresponding author: Hitler Louis, phone: +86 15 001075832, e-mail address: louismuzong@gmail.com; louis@nanoctr.cn

ARTICLE INFO

Article history:
Received: October 18, 2018
Accepted: December 25, 2018
Published: January 28, 2019

Keywords:
1. metal complex
2. molecular catalyst
3. photocatalysis
4. mechanism
5. CO_2 electrochemical

ABSTRACT: Significantly, global warming which is caused by CO_2 emission and energy shortage are global problems resulting from artificial photosynthesis because it required many functions (light harvesting, Z water, and oxidation scheme). Therefore, photocatalytic systems development for CO_2 reduction is germane in this field. Metal complexes molecular catalyst have become prevalent homogeneous catalysts for carbon dioxide (CO_2) photocatalytic reduction since it was initially known as CO_2 reduction catalysts in the 70s and the 80s, while utmost part involved macrocyclic cobalt(II) and nickel(II) complexes. This review article presents a broad understanding on some active catalysts recently reported as a metal complex molecular catalytic schemes for CO_2 reduction, alongside catalytic activity, stability, selectivity under electro-reduction, and photoreduction circumstances. The progress of *in situ* spectroelectrochemical methods, typically supported via theoretical calculations, helped to access this know-how by providing information which enabled researchers to acquire more in-depth perception into unveiling the catalytic reaction and mechanisms intermediates.

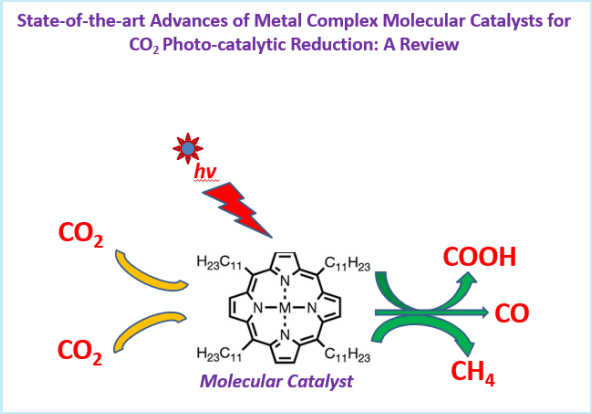

1. Introduction

The increasing level of atmospheric CO_2 concentration and fossil resources diminishing are sources of global environmental problems, hence, restoring environmental paradigm requires: atmospheric CO_2 level monitoring and renewable energy sources exploration for alternative uses CO_2 to value-added products[1-3]. For instance, CO_2 conversion for other uses (e.g., fuel or chemical feedstock compounds) could fundamentally reduce CO_2 emissions and fossil fuel consumption causing climate change and other related environmental problems[1]. Moreover, the reliability of electrocatalytic reduction of CO_2 method has been reported, because: (i) operates under ambient conditions and (ii) could exert electricity produced from renewable energy sources[2]. Selective photocatalytic CO_2 reduction to CO is one promising process because CO is an essential feedstock chemical for liquid hydrocarbons and methanol production[4]. Several materials (e.g.

Eclética Química Journal, vol. 44, n. 1, 2019, 11-39
ISSN: 1678-4618
DOI: 10.26850/1678-4618eqj.v44.1.2019.p11-39

metals - Cu, Au, Ag, and Zn)[5-8], metal oxide semiconductors – ZnO, SnO_2[9, 10], metal dichalcogenides – MoS_2 and WSe_2[11, 12], and transition-metal-based molecular complexes: Mn-, Fe-, Co-, Ni-, Cu-, Ru-, and Re-based complexes[13-15], have been utilized for catalyzing electro-reduction of CO_2 to liquid fuel hydrocarbons. It has been widely known and generally accepted that there are three significant steps in photocatalysis: solar light harvesting, charge separation and transportation, and surface reactions. By using the CO_2 reduction catalysts, significant progress has been made in optimizing the first two steps as they involve the same issues in solar-driven water splitting and CO_2 reduction reaction systems[16-22]. The primary difference between these two photoconversion systems is the surface reaction of charge carriers (electrons for reduction and holes for oxidation). Scientists have devoted an enormous effort in order to improve the efficiency of the third step in solar water splitting, much more than in CO_2 photoreduction[23, 24].

Generally, two types of materials (homogeneous metal complexes [coordination and organometallic complexes] and solid materials) are revealed in recent CO_2 reduction catalyst studies. At the same time, while acknowledging the significance of former approach, our interest in this review would address the mechanisms and benefits of metal complex molecular catalysts; a common model for fine-tuning reactivity by ligands synthetic modifications. Molecular catalysts attributes must include the ability to store multiple reducing equals over-mediated multi-electron/multi-proton transformations essential for catalytic CO_2 reduction. This can be achieved either by reducing the metal center, which then obliges a proficient ligand field to stabilize the reduced metal ions or by lessening the ligand scaffold, with the metal operating as a mediator for electron relay[25-28]. Nonetheless, it is challenging to transform a "conventional" catalyst into an electrochemical type owing to preconditions and design rules/set[26, 27]. Notably, the catalyst conduction band edge requires a suitable range, while the catalyst reduced form is adequately stable, and the chemical step is obtainable under the desired electrolysis conditions. Expectedly, the operating state of homogeneous electrocatalyst should adjoin the thermodynamic reaction potential of the proposed catalysis, while fast chemical step kinetics is mandatory for rapid turnover frequency. For metal-organic compounds, these factors are adjustable consequent to anticipated electrolysis conditions of an appropriate metal choice and ligand tuning optimization. In the last few decades, remarkable advancement has been achieved both in the electrocatalytic performance optimization as well on mechanistic aspects.

2. Background of molecular catalyst

2.1 Principles

Most electrochemical reactions are conducted in a pair, indicating that reaction at the anode (anodic reaction) is paired with a reaction occurring at the cathode (cathodic reaction) in the photoelectrochemical cell (PEC). The co-reaction of two electrochemical, separately provides valuable, important product or intermediate for chemical synthesis, and constitutes a universal sustainable production plan for chemicals[29]. Past studies have recorded weighty examples for paired electro-organic syntheses[29-31]. However, the most prevalent paired process is chloro alkali electrolysis. Such a method can be practical to recover the energy efficiency and the atom economy in comparison to distinctly conducted processes. Achieving a maximum Faradaic efficiency (200%) is realizable since the passed electric charge is primarily used twice. However, in CO_2 reduction, the conventional approach for up-scaled reactors is the coupling to water oxidation (oxygen evolution reaction, OER)[32-36].

Electrocatalysts *sensu lato* are perfect electron transfer agents that function near the thermodynamic potential of the intended driven (products/substrates). Because, the overpotential is the difference between the applied potential ($V_{applied}$) necessary to produce certain current density at a time t, and the thermodynamic potential (E^o) of the studied system, direct electrochemical CO_2 reduction on virtually all electrode surfaces requires a tremendous over-potential, which consequently decreases the conversion efficiency because the amount of voltage applied is greater as compared to the thermodynamic required voltage. Interestingly, at this state, both thermodynamic and kinetic considerations are essential. Apparently, the function of catalysts is to minimize overpotentials and for that, their development is based on the following requirements: (a) to possess formal potentials (E^o ($C^{atn+/0}$), well matched to reactions

Eclética Química Journal, vol. 44, n. 1, 2019, 11-39
ISSN: 1678-4618
DOI: 10.26850/1678-4618eqj.v44.1.2019.p11-39

[E^o] (products/substrates), and (c) appreciable constants rate, for substrates chemical reduction to products at the present state. In addition, the heterogeneous rate constant for electrocatalyst reduction at the electrode surface must be high[37]. A general method for an electrocatalytic system is presented in Figure 1.

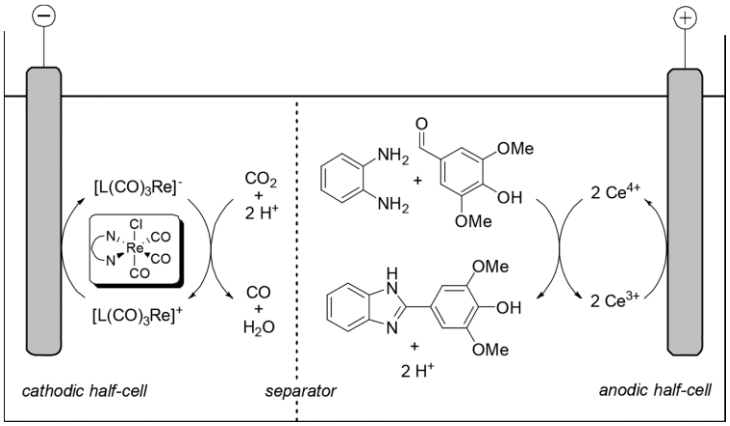

Figure 1. Diagrammatic illustration of a paired electrolysis relating cathodic CO_2-to-CO conversion catalyzed with a Re complex and anodic synthesis of a 2-substituted benzimidazole mediated by ceric ammonium nitrate[38]. Modified by the authors.

2.2 Carbon dioxide coordination Chemistry

2.2.1 Electronic structure of CO_2

The electrocatalytic CO_2 reduction is activated by the interactions of the active form of the catalyst and the substrate molecule through a process of activation. Carbon dioxide (16e^- molecule), belongs to $D_{\infty h}$ symmetry group with linear geometry at the ground state or gaseous phase. Regardless the molecular nature (nonpolar molecule and chemical stability), it encompasses two polar bonds, with two orthogonal orbital (π) sets. Previously CO_2 is assumed to be a poor ligand, however topical scientific studies on CO_2 has improved this understanding which are the display of various coordination mode and several coordination sites in its complexes. The carbon atom (LUMO orbital), has a Lewis acid character and can be described as an electrophilic center, while the oxygen atoms (HOMO orbitals) are weak Lewis bases and defined as nucleophiles[39]. Noteworthy, most CO_2 catalytic reactions involve a concurrent acid-base activation, with the carbon atom and one of the oxygen atoms tangled in the interface with the metal[40]. The two double bonds include π electrons that can interrelate per transition metals electrons in a Dewar – Chatt – Duncanson bonding scheme Figure 2[41]. When the CO_2 LUMO orbitals are engaged (through electron transfer), the least energy state and a bent geometry are equivalent, reflected in the bond length increase, bond angle decrease, and a negative charge determined by the degree of CO_2 adsorption and activation.

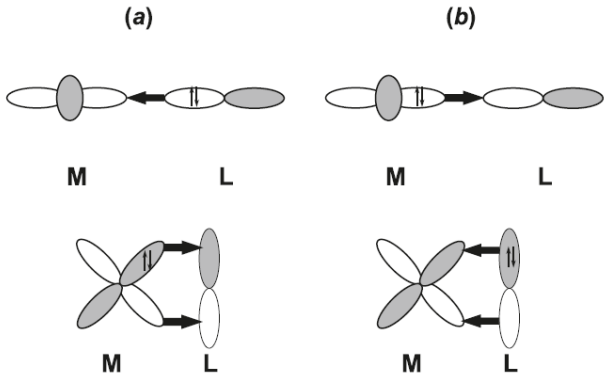

Figure 2. Schematic representation of (*a*) the Dewar–Chatt–Duncanson model and (*b*) the reversed Dewar–Chatt–Duncanson model[41]. *Reprinted with permission from Goedecke, et al., The Dewar–Chatt–Duncanson model reversed—Bonding analysis of group-10 complexes [(PMe3)2M–EX3] (M = Ni, Pd, Pt; E = B, Al, Ga, In, Tl; X = H, F, Cl, Br, I), Can. J. Chem. 87 (10) (2009) 1470-1479, © Canadian Science Publishing.*

2.2.2 Carbon monoxide binding modes

There are four basic CO_2 coordination approaches [(C, O), and binding modes [Figure 3, ref. 39]. The coordination mode involves a significant charge transfer between a metal orbital

Eclética Química Journal, vol. 44, n. 1, 2019, 11-39
ISSN: 1678-4618
DOI: 10.26850/1678-4618eqj.v44.1.2019.p11-39

and the antibonding CO_2 orbital. This bonding mode is made easier via additional weak interaction between one or two CO_2 oxygen atoms with a Lewis acid center positioned in the metal coordination domain and more partial with nucleophilic (electron-rich) metals. The η^1-CO_2 complexes are not strong; mostly, their isolation entails glove box or Schlenk techniques, exclusion of oxygen and water[40-42]. Following past records of Herskovitz[43, 44] on η^1 complexes, it becomes requisite to pressurize the system with CO_2 in order to attain complexes (iridium and rhodium). Nevertheless, ligand displacement does not occur in the forming process of these compounds. In the (C, O) bonding mode, there is a double bonding structure involving bond from the CO_2 orbital to an empty metal orbital, alongside a "back-bonding" from a filled d_{xy} metal orbital to the empty CO_2 orbital. Aresta and Nobile[45] reported the η^2 complex $[Ni(CO_2)(PCy_3)_2]$ made by reaction of $Ni(PCy_3)_3$ or $[Ni(PCy_3)_3]N_2$, in toluene, with CO_2 at atmospheric pressure and obtained as toluene solvate. The η^1 (O) end-on coordination mode is ideal with electron poor metals, and the CO_2 molecule may persist as linear or bent weakly. The (O, O) coordination mode can be defined as a metal carboxylate with an ionic bond and regularly encountered with alkali or alkaline-earth metals or, with metal surfaces in the CO_2 adsorption, for instance. Also, η^2-CO_2 complex synthesis was conveyed by Karsch[46] from the reaction of $Fe(PMe_3)_4$ with CO_2 in pentane; a second product, $Fe(PMe_3)_3(CO)(CO_3)$ was likewise attained. Recently, features of the complex $Fe(CO_2)(depe)_2$, fully characterized by Komiya *et al.*[47], buttressed the formulation of the first compound (Karsch[46]).

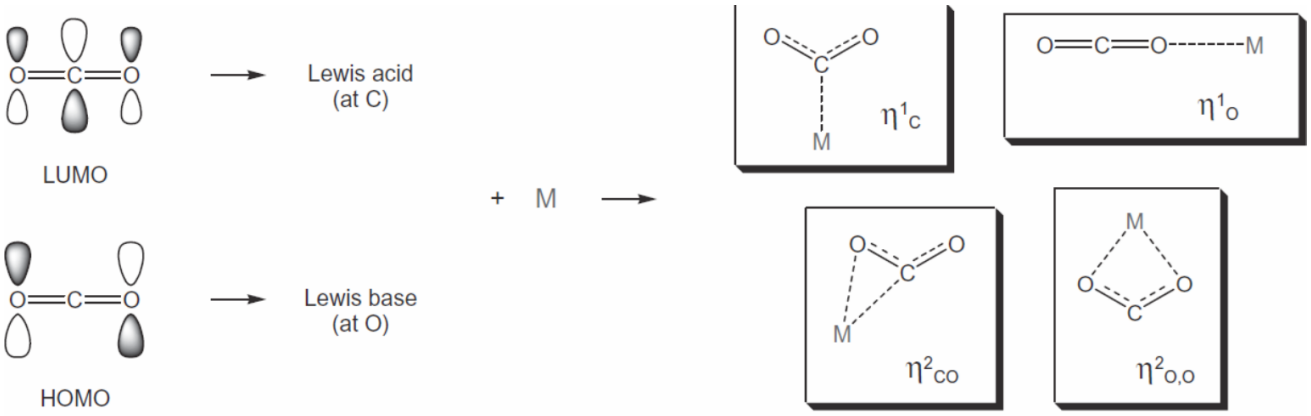

Figure 3. CO_2 coordination modes to a single metal center[39-42].

2.3 Recent Advances of CO_2 Reduction using Molecular Catalyst

2.3.1 Iron-based Molecular Catalyst

As previously explained, electrochemical CO_2 reduction to hydrocarbon fuel plays a significant part in climate change and energy cycle[48]. For instance, in the Fischer-Tropsch process carbon monoxide and hydrogen can be converted to liquid fuels. Molecular catalysts (homogenous or heterogeneous) in electrochemical or photochemical conditions are typically useful in the field[49]. In past years, iron porphyrins and metal-organic structures have received vast attention for electrocatalytic and photo electro-catalytic CO_2 reduction[50]. Applications of various modern methods and modification through synthesis to enhance the reactivity and product selectivity afforded homogeneous electro-catalysts to be one of the preferred approaches. Past results of Taheri *et al.*[51] on "an iron electrocatalyst for selective reduction of CO_2 to formate in the water" stated that with low applied overpotential, formate is produced with a high current density and Faradaic efficiency (96%). Besides, those studies explicated catalysis mechanism by means of cyclic voltammetry, and structurally categorized a key reaction intermediate, that is the reduced hydride.

Combination of investigational data in MeCN/H_2O (95:5) and aqueous solution point to a mechanism for CO_2 reduction where the electrocatalyst (Fig. 4) is reduced from $\mathbf{1}^-$ to $\mathbf{1}^{2-}$ and then protonated to produce $(H-\mathbf{1})^-$. A further selective reaction of $(H-\mathbf{1})^-$ with CO_2 to yield a C−H bond resulted in formate.

Eclética Química Journal, vol. 44, n. 1, 2019, 11-39
ISSN: 1678-4618
DOI: 10.26850/1678-4618eqj.v44.1.2019.p11-39

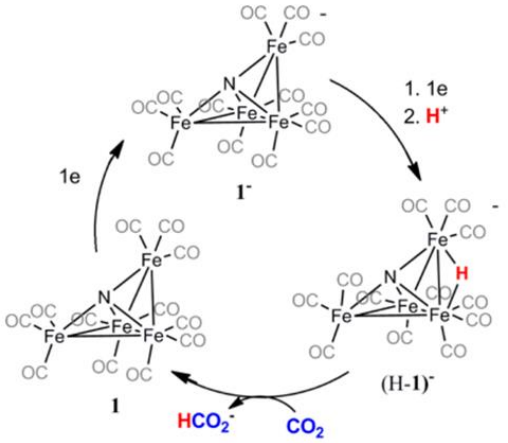

Figure 4. Projected Mechanism for Reduction of CO_2 to Formate by $\mathbf{1}^-$ in the Existence of Protons[51]. *Reprinted with permission from Taheri et al., An iron electrocatalyst for selective reduction of CO_2 to formate in water: including thermochemical insights, ACS Catalysis 5 (12) (2015) 7140-7151. ACS Catal. 2015, 5, 7140−7151. Copyright (2015) American Chemical Society.*

Ambre *et al.*[52] explored the "molecular engineering for effectual and discriminating iron porphyrin catalysts for the electrochemical reduction of CO_2 to CO". Here, ester groups (*para*, *meta*, and *ortho* positions) of Fe-porphyrin were introduced and set iron porphyrins Fe-*p*E, Fe-*m*E, and Fe-*o*E. The electrochemical reduction of CO_2 to CO by these catalysts was studied. The Faradaic efficiency [(FE) - exclusive 65% and quasi-exclusive 98%] for CO was accomplished by Fe-*m*E and Fe-*o*E in CO_2 saturated electrolyte with addition of 2 mol L^{-1} H_2O, after 2 h bulk electrolysis. Also, the *meta*-substituted derived (**FE-*m*E**) is extremely selective for CO production giving FE (65%) lacking competitive H_2 production while the *para* substituted (**Fe-*p*E**) generated only H_2 (FE, 84%) as a key product of bulk electrolysis.

The cyclic voltammograms (CVs) results of these Fe porphyrins specify that Fe-*p*E, Fe-*m*E, and Fe-*o*E in DMF exhibited distinctive iron porphyrins redox behaviors. Notably, the $E(Fe^{I/0})$ of Fe-*o*E is apparently more negative than those of Fe-*p*E and Fe-*m*E, perhaps consequence of its dipole. Therefore, the Fe^0 species of Fe-*o*E is the most robust reducing catalyst between these four Fe porphyrins. Congruently, Savéant and co-workers also discussed that the reduction of CO_2 is simplified by Fe(0) species at Fe(I)/Fe(0) redox wave under CO_2 atmosphere[53-55].

Further, Rao *et al.*[56] studied the "visible-light-driven methane formation from CO_2 with a molecular iron catalyst". They observed functionalization of iron tetraphenylporphyrin complex with trimethylammonio groups, which is the most common, competent and selective molecular electrocatalyst for CO_2 conversion to CO[57-59]. This catalyst is also able to catalyze the eight-electron CO_2 reduction to methane upon distinguishable light radioactivity at ambient temperature and pressure. In addition, the catalytic system functioned in an acetonitrile solution covering a photosensitizer and sacrificial electron donor and works stably over several days. Direct CO_2 photoreduction reaction produces CO as the principal product, nonetheless, a two-pot method that first reduces CO_2 to CO and then reduces CO to methane with a selectivity (ca. 82%) and quantum yield (0.18%). Figure 5 presents conceivable mechanism illustration based on obtained results and experimental considerations, including the assumption of formyl intermediate[60, 61], which could be steadied through space interactions between the trimethylammonium group's positive charges and fractional negative charge on the CHO species bounded to the metal.

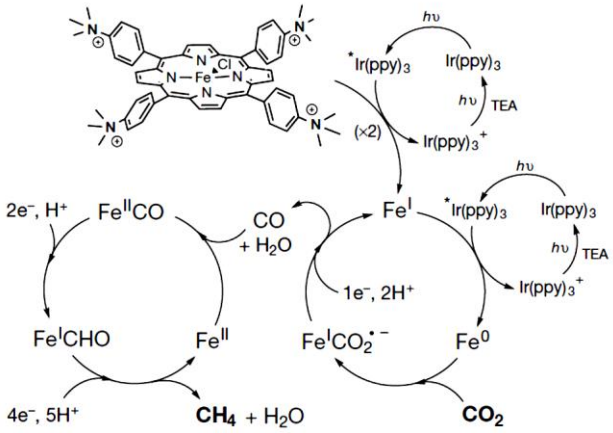

Figure 5. Illustration of the mechanism for CO_2 reduction to CH_4[56]. *Reprinted with permission from Rao et al., Visible-light-driven methane formation from CO_2 with a molecular iron catalyst, Nature 548 (2017) 74-77. Spinger Nature and Copyright (2017) Clearance Center.*

The description of the suggested mechanism includes; the reduction of proceeding Fe^{3+} porphyrin (top left) with three electrons to the catalytically active Fe^0 species. The CO_2 is reduced with Fe^0 species, regenerating FeI due to electron

Eclética Química Journal, vol. 44, n. 1, 2019, 11-39
ISSN: 1678-4618
DOI: 10.26850/1678-4618eqj.v44.1.2019.p11-39

transfer from the excited photosensitizer (right-hand side cycle). The resulting CO binds to Fe^{2+} and further lessened with six electrons (transferred from the excited sensitizer) and protons to make methane, from a guessed FeI-formyl (FeICHO) intermediate (left-hand side cycle).

Lately, Pan and co-workers[62] experimented the "active sites of CO_2 reduction on nitrogen-coordinated and atomically isolated iron and cobalt catalysts." They observed that Fe–N_4 sites are inherently extra efficient than Co–N_4 sites in M–N–C catalysts for CO_2 reduction to CO with high FE, more positive onset potential, and ample. Likewise, they computationally acknowledged (Figure 6) that the edge-hosted (M–N_{2+2}–C_8) sites bridging two armchair-like graphitic layers were dynamic moiety for the CO_2RR. Unambiguously, the M centers and C atoms, floppy bonds and following N are the vigorous *CO and *OH adsorb sites in the C–O bond cleavage throughout the CO_2RR, correspondingly.

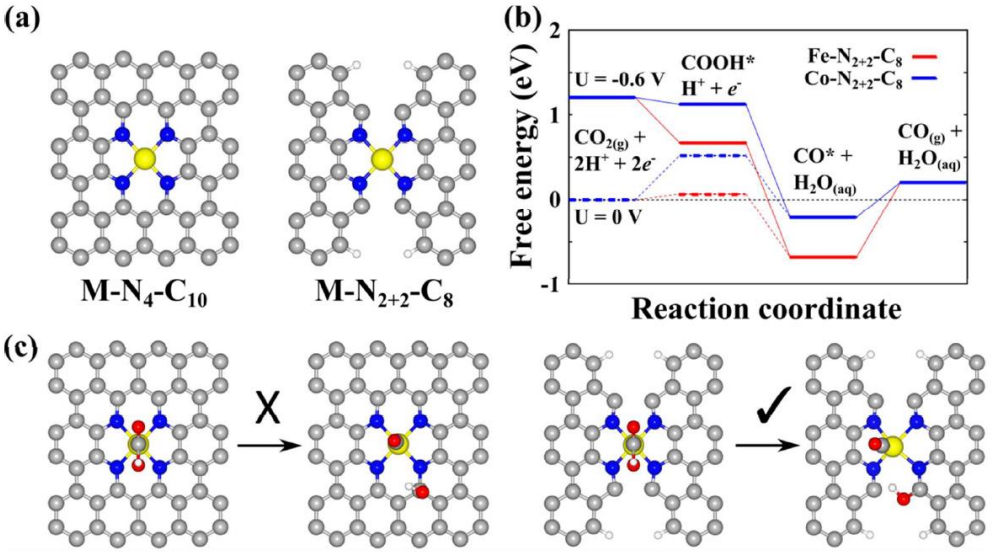

Figure 6. Atomic structure of M–N_4–C_{10} and M–N_{2+2}–C_8 (M=Fe or Co) active sites. (b) Calculated free energy evolution of CO_2 reduction to CO on M–N_{2+2}–C_8 sites under useful electrode potential (U) of 0 V and −0.6 V. (c) The initial and final state for the COOH dissociation reaction on M–N_4–C_{10} and M–N_{2+2}–C_8 sites. In the figure, the gray, blue, yellow, red, and white balls represent C, N, M, O, and H atoms, respectively[62]. *Reprinted with permission from Pan et al., Unveiling Active Sites of CO_2 Reduction on Nitrogen-Coordinated and Atomically Dispersed Iron and Cobalt Catalysts, ACS Catal. 8 (4) (2018) 3116-3122. Copyright (2018) American Chemical Society.*

The positional secondary organization dependence sphere groups on the reactivity of a conserved chief iron porphyrin core for electrochemical CO_2 reduction were investigated by Nichols *et al.*[63]. Thereby, four positional isomers (Figure 7) were synthesized, changing the position of the second-sphere amide group *ortho-* and *para-*, likewise proximal and distal, to the porphyrin plane.

In an atmosphere of CO_2 and in existence of phenol (acid source), CO_2 reduction catalytic responses suggestive is examined using cyclic voltammetry for all catalysts. Comparatively, when phenol (100 mmol L^{-1}) was used, Fe–ortho-1-amide display a catalytic onset that is somewhat more positive than Fe–ortho-2-amide, while both evinces meaningfully higher catalytic responses than the equivalent para-functionalized positional un-functionalized Fe-TPP.

For a better understanding of CO_2 reduction catalyzed by this series of amide-functionalized porphyrins, the pragmatic constants rate determined by FOWA were reviewed as a function of phenol and CO_2 concentration. All four functionalized catalysts reveal first-order dependence on phenol concentration under pseudo-first order circumstances. Fe–ortho-2-amide has the most momentous experimental constants rate of all catalysts studied. Nonetheless, displays non-linearity at higher phenol concentrations, probably as a result of catalyst inhibition or local depletion of CO_2. The Fe–ortho-1-amide has the next highest values (K_{obs}), trailed by Fe–para-2-amide while

Eclética Química Journal, vol. 44, n. 1, 2019, 11-39
ISSN: 1678-4618
DOI: 10.26850/1678-4618eqj.v44.1.2019.p11-39

Fe–para-1-amide is the least. To appraise the catalytic efficacy, it is mandatory to examine the overpotential (η) vs. log (TOF) relationships exhibited by the catalytic Tafel plot[64]. Operative catalysts function with higher TOFs at lower overpotentials (upper left portion of such plots. Fe–ortho-2-amide demonstrate higher TOFs above all over potential values than Fe–ortho-1-amide that exhibits higher TOFs compared to Fe-TPP and both *para*-substituted porphyrins. The values at the peak of the curves depict the maximum turnover frequency realizable at large over potential. It crucial to emphasize the difference in E_{0cat} values amongst catalysts when aiming to resolute optimal second-sphere pendant location queries. Previously[65, 66], the electrochemical CO_2 reduction driving force is habitually pretentious by electron retreating or bequeathing substituents on the porphyrin aryl rings (E_{0cat}). In such event, a linear scaling relationship among log(TOF_{max}) and its observations (E_{0cat}), moreover, larger TOFs is achieved wherever there are catalysts with high negative values (E_{0cat}). Nonconformity arises when second-sphere interactions either inhibit or promote catalysis, as previously recorded for electrostatic effects[67].

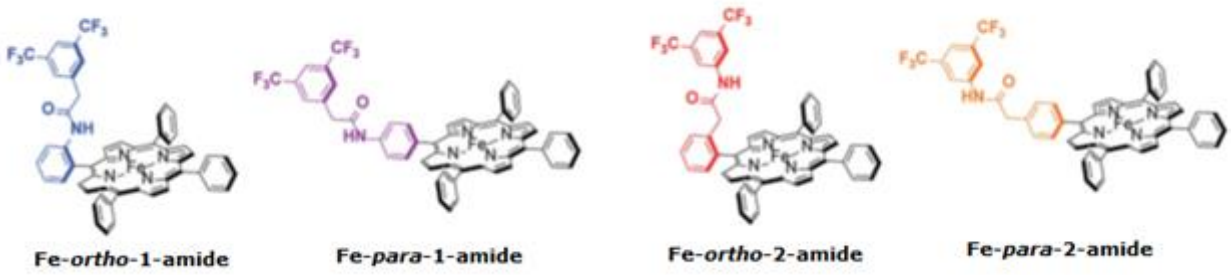

Figure 7. Positional isomers of amide-functionalized iron tetraphenylporphyrins[63]

2.3.2 Zn-based Metal Complex Molecular Catalyst

In terms of price, abundance, and toxicity of the metal center, the use of zinc-based systems is of significant interest. Hence, it is amazing that only a handful examples of zinc catalyzed hydrosilylation of CO_2 have been reported in literature: two cationic, N-heterocyclic carbene (NHC) zinc complexes, a dicationic NHC-stabilized zinc hydride cluster, including the tris(thiopyridyl) methane based [Tptm] ZnH and the tris[(1-isopropylbenzimidazol-2-yl)dimethylsilyl] methane-based [TismPriBenz] ZnH complexes catalytically reacted with CO_2[68-72]. The synthesis and evaluation of two new Zn(II) complexes for their ability to stimulate and reduce CO_2 have been stated by Donovan *et al.*[73]. The electrochemical characteristics of dichloro[phenyldi(2-pyridyl)phosphine-κ^2-*N*,*N*'] zinc(II) and dichloro[diphenyl-(2-pyridyl)phosphine-κ^1-*N*]zinc(II) complexes are contrasted with cyclic voltammetry.

To explore the reactivity of these complexes (dichloro[phenyldi(2-pyridyl)phosphine-κ^2-*N*,*N*'] zinc(II) and dichloro[diphenyl-(2-pyridyl)phosphine-κ^1-*N*]zinc(II)) with CO_2, samples of each complex were exposed to bubbling CO_2 as 0.20 mol L^{-1} solutions in THF. Afterward, the solid materials isolated from these solutions were placed on KBr windows via solvent evaporation at CO_2 room temperature. Comparatively, the results showed that dichloro[phenyldi(2-pyridyl)phosphine-κ^2-*N*,*N*'] zinc(II) complex lacks a continuous CO_2 adduct form since no changes were observed in the IR spectrum while dichloro[diphenyl-(2-pyridyl)phosphine-κ^1-*N*]zinc(II) complex showed a novel stretching band (1726 cm^{-1}) after 30 min at room temperature reaction time. This implies the formation of a novel compound species, **2-CO_2**. Cyclic voltammetry was used to confirm if dichloro[diphenyl-(2-pyridyl)phosphine-κ^1-*N*]zinc(II) complex could reduce the overpotential required to reduce CO_2[74]. In the ambient CO_2 atmosphere, the reduction peak onset shifted anodically (approximately 0.6 V) when a potential negative bias was utilized to dichloro[diphenyl-(2-pyridyl)phosphine-κ^1-*N*]zinc(II) complex. There is concordance between the voltammogram and the IR data as it advocates the existence of CE mechanism. Intriguingly, carbon monoxide

Eclética Química Journal, vol. 44, n. 1, 2019, 11-39
ISSN: 1678-4618
DOI: 10.26850/1678-4618eqj.v44.1.2019.p11-39

evolution was ascertained in the mass spectra acquired before and after bulk electrolysis. The electrolysis cell headspace was determined for gas composition in an airtight syringe and injected into a GC/MS instrument. The attained spectrum prior to controlled potential electrolysis (CPE), showed the superseding peak (44 *m/z*) assigned to CO_2 with the other negligible peaks in the spectrum result. Besides, the CO_2 obtained was an insignificant product in the mass spectrum and topmost (28 *m/z* is leading) after 4 hours of CPE. Summarily, it is evident that dichloro[diphenyl-(2-pyridyl)phosphine-κ^1-*N*]zinc(II) complex is the first organometallic Zn complex that improves the CO_2 electrochemical conversion to CO and sinking the required overpotential (approximately 0.6 V). Moreover, this transformation is earned at a glassy carbon electrode; more desirable compared to expensive Pt or Pd alternatives often used for electrocatalysis of this kind.

Wu *et al.*[75] reported heterogeneous zinc−porphyrin complex (zinc (II) 5,10,15,20-tetramesitylporphyrin) as an electrocatalyst that consigns a relatively high turnover frequency (14.4 sites^{-1}s^{-1}) and a Faradaic efficiency (95%) for CO_2 electro-reduction to CO at −1.7 V *vs.* usual hydrogen electrode in an organic/water mixed electrolyte. The PorZn electrodes were studied for electrochemical CO_2 reduction at different potentials in a CO_2-saturated solvent system including 0.1 mol L^{-1} tetrabutylammonium hexafluorophosphate hexafluorophosphate ($TBAPF_6$) in DMF/H_2O. The fractional current CO production densities and matching Faradaic efficiencies at various potentials are represented (Figure 8A, left). Positive potentials above −1.4 V *vs.* SHE, resulted in H_2 as the only product. CO_2 conversion to CO observation begins at −1.4 V, with a CO 22% Faradaic efficiency. Notably, applications of more negative potentials are corresponded to increase in both the current density and CO Faradaic efficiency. The supreme CO Faradaic efficiency (95%, −1.7 V *vs.* SHE) with a current density (ca. 2.1 mA/cm^2). Equally, the CO Faradaic efficiency and total current density can be reserved (at least 4 hours at −1.7 V, Figure 8B, left). Certain that Zn metal is an active recognized catalytic for electrochemical CO_2 reduction to CO[76-78], it is important to ignore the metallic Zn formation, and its catalyzing reaction.

To observe oxidation state vagaries and Zn center electronic structure in electrochemical CO_2 reaction situations, *in situ* and operando XAS extents was conducted with the reaction cell previously reported[79]. This method has been magnificently used to scrutinize the Co oxidation state in a solid-state (cobalt−porphyrin-based catalyst material) in electrocatalysis[80]. No obvious variations in the Zn K-edge X-ray absorption close to edge structure (XANES) spectra are detected as the active electrode potential is tuned from open circuit voltage (OCV, −1.7 V *vs.* SHE) (Figure 8A, right) and thereafter to +0.2 V *vs.* SHE, depicting no changes of Zn center oxidation state in the PorZn catalyst at the tested potential range. The high-quality data afforded us a clearer understanding of the PorZn local structures. As presented in Figure 8B (right), slight variations in the Zn coordination number and bond distances are recorded at the examined potentials and during electrolysis. The inconsequential alterations in the Zn local structure could be attributed to the reduction of the porphyrin ligand or binding of molecules on the Zn site. This shows that the Zn center is influential to the PorZn catalytic activity, despite that it is still redox-innocent during electrocatalysis.

The PorZn porphyrin ligand is therefore likely to be the impetus for the two-electron reduction of CO_2 to CO. The PorZn CV in saturated electrolyte shows a reduction wave that begins near −1.4 V *vs.* SHE, corresponding with the CO_2 reduction to CO observation at the potential. The cyclic voltammograms in Ar-saturated electrolyte exhibit a comparable wave linked with PorZn reduction, perhaps joined with protonation[81-84]. The utmost surprising alteration among the two CVs is the reversing wave pattern. The CV in CO_2-saturated electrolyte presents anodic wave that is weak (about −1.45 V) equivalent to the reduction wave (about −1.6 V). In contrast, the CV in Ar-saturated electrolyte presents three anodic waves (about −1.53 V, −1.17 V, and −0.43 V *vs.* SHE). Similar event (three anodic waves) was recorded in an investigation of zinc(II) 5,10,15,20-tetraphenylporphyrin studied at the same scan rate[83]. Following precedent literature[83], these anodic waves are presumed to conform with subsequent oxidation and deprotonation of the reduced porphyrin ring. For deeper understanding in PorZn-catalyzed CO_2 reduction, Wu and co-workers conducted PorZn chemical reduction using solution under inert situations and adopt one or two equals of sodium naphthalene in tetrahydrofuran (NaNap, ca. −2.4 V *vs.* SHE in THF[85]) as the reducing agent. The reduced PorZn

Eclética Química Journal, vol. 44, n. 1, 2019, 11-39
ISSN: 1678-4618
DOI: 10.26850/1678-4618eqj.v44.1.2019.p11-39

species display absorption bands at 710, 820, and 920 nm in the UV−Vis spectra, which are features of transiently generated zinc−porphyrin compounds with reduced ligands[81, 86]. Upon exposure of the reduced PorZn species to air, the rapid PorZn renaissance was reported in the UV−Vis spectroscopy. Thus far, the wavering of these reduced species has precluded full characterization. This experiment discloses the first molecularly structured Zn-based catalyst for electrochemical CO_2 reduction to CO with significant product selectivity. The Zn(II) center, implies redox-inactive though intrinsic to the catalysis, which separates the studied catalyst from transition metal-based molecular catalysts previously reported.

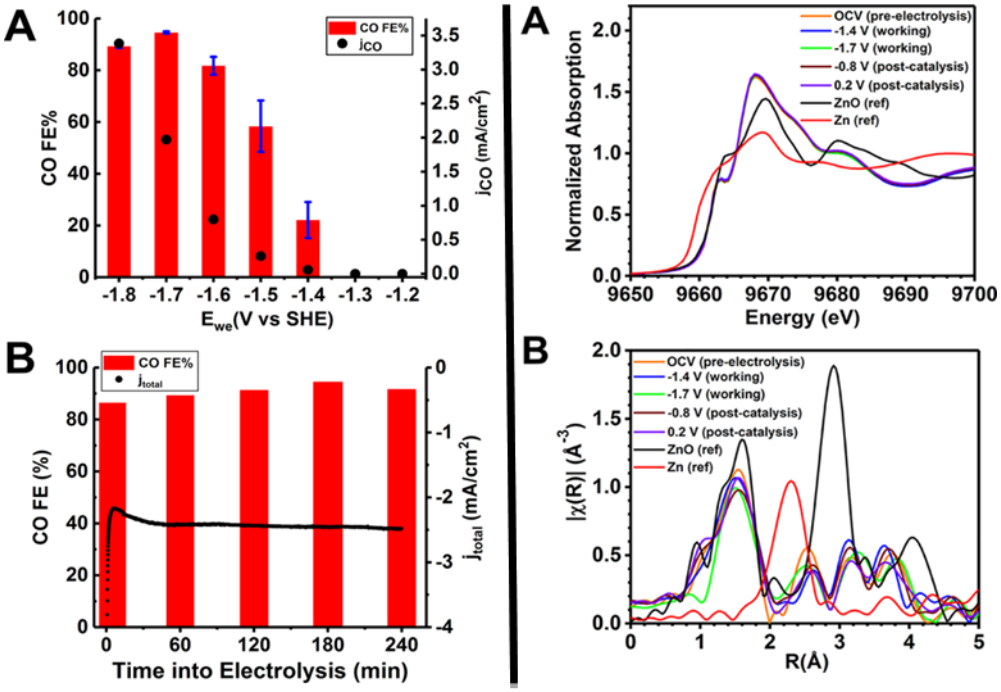

Figure 8: (Left) Electrochemical CO_2 reduction catalyzed by the PorZn electrode in 0.1 mol L^{-1} $TBAPF_6$ DMF/H_2O solution. (A) CO Faradaic efficiencies and CO partial current densities at different potentials averaged from three measurements. (B) CO Faradaic efficiencies and total current densities after 5, 60, 120, 180, and 240 min of electrolysis at −1.7 V *vs.* SHE. (right) (A) Zn K-edge XANES spectra and (B) Fourier transforms of Zn K-edge EXAFS spectra of the PorZn catalyst electrode at different potentials (V *vs.* SHE)[75]. *Reprinted with permission from Wu et al., Electroreduction of CO_2 Catalyzed by a Heterogenized Zn-Porphyrin Complex with a Redox-Innocent Metal Center, ACS Central Science 3 (8) (2017) 847-852. Copyright (2017) American Chemical Society.*

Wang *et al.*[87] studied aqueous electrocatalytic reduction of CO_2 of several synthesized ZIF–8 nanomaterials, having uncommon properties e.g., large surface area, uniform pore size, well-defined morphology, and strong coordination. Upon CO_2 electrochemical reduction, ZIF–8 nanocomposites are substantiated to be effective and proposed (ZIF–8 metal nodes) as active catalysis sites. The synthesis of CO_2 reduction electrochemical employing the nanomaterials (ZIF–8) braced on glassy carbon (GC) electrodes was assessed using CV in 0.5 mol L^{-1} NaCl aqueous solution. CV traces of different ZIF–8 materials in Ar and CO_2 exhibit magnified current and positively shifted beginning potential of catalysis in CO_2 for both nanomaterials (ZIF–8^{SO4} and ZIF–8^{NO3}) For ZIF–8^{SO4}, the positive potential shift is ca. 400 mV and ZIF–8^{AC} presents slightly less current in CO_2 compared to Ar. Notwithstanding, the current of ZIF–8^{AC} decreases a bit, yet distinguishable from other two materials (ZIF–8^{SO4} and ZIF–8^{NO3}) at the surface loading uniformity. Further, when combined with electrolysis results, ZIF–8^{AC} demonstrated high current for hydrogen evolution, and not CO_2 reduction.

The Controlled-potential electrolysis (CPE) were observed under CO_2 to understand the

Eclética Química Journal, vol. 44, n. 1, 2019, 11-39
ISSN: 1678-4618
DOI: 10.26850/1678-4618eqj.v44.1.2019.p11-39

distribution of product and the FE. The potential utilized current between –1.4 V and –1.9 V *vs.* SCE using similar electrode. For gaseous analysis and liquid phase products, gas chromatography (GC) and nuclear magnetic resonance spectroscopy (NMR) was applied. Three discoveries were reported: (i) all ZIF-8 materials, (ii) important products (H_2 and CO) and (iii) only a small amount of formate in the liquid phase was discovered. The used potential increase the FE for CO primarily increases till maximum attainment, and then lessening with further utilized potentials Various CO Faradaic efficiency were obtained (highest = ZIF–8^{SO4}[65.5%], ZIF–8^{NO3}[69.8%] & ZIF–8^{AC} [57.7%] at –1.8 V *vs.* SCE, however, ZIF–8^{SO4} displays the most extensive potential range appropriate for CO production (–1.5 to –1.9 V *vs.* SCE. The current densities of H_2 and CO products for ZIF-8 materials at –1.8 V *vs.* SCE has been also investigated[87]. The heightened partial CO current density justified that ZIF–8^{SO4} is a highly efficient catalyst for CO_2 reduction compared to ZIF–8^{NO3} and ZIF–8^{AC}.Many synthesized ZIF–8 nanocomposites were proven to be impressive CO_2 reduction catalysts. Through zinc sources regulation, ZIF–8 chemical reactivity can be modulated, and ZIF–8^{SO4} generates excellent CO selectivity. Likewise, the electrolyte performs a vital role for high CO selectivity. The Cl^- anion improves and yields the best CO_2 reduction reactivity, probably due to superficial anion exchange and small hydrated range. These observances propound ZIF-8s as effective electrocatalysts for CO_2 reduction.

2.3.3 Mn-based Metal Complex Molecular Catalyst

The most persistent manganese oxidation state occurs in +2, +4, and +7 of the compounds complete range formed by manganese. The Mn^{+7} oxidation state is sturdy, frequently lessened to Mn^{+2}. The oxidation state of Mn^{+1} is less common, but normally ensues within manganese-based organometallic complexes; d^6 Mn^I tricarbonyl complexes have become important in the catalysis field[88, 89]. Typically, complexes like the archetypal *fac*-[Mn(bpy) $(CO)_3Br$] uncover a HOMO controlled by a Mn 3d-orbital and a diimine-based LUMO. The electronic and photophysical character state of analogous Mn^I complexes can be better adjusted through diimine ligand chemical structure modification hence adapting the LUMO energy. Application of manganese as a catalyst is due to chemical similarities with rhenium (same group, oxidation states, and geometries). Nonetheless, manganese is 1.3 million times more abundant in the Earth's crust than rhenium[90].

There are several reviews on transition metals and manganese-based systems for CO_2[91-94] until recent review (Sinopoli *et al.*[90]) which unveiled the efficiency, feature and strategy of Mn carbonyl schemes for CO_2 electro- and photoreduction. In the same way, Stanbury and colleagues[95] reported in a comprehensive survey of all the Mn carbonyl systems reported as being active catalysts for CO_2 reduction, based on activity, stability, and selectivity under electro-reduction and photoreduction circumstances. In their review, they uncovered that Mn-based carbonyl complexes display an elevated capacity for CO_2 catalysis through electro-, photo- or photo electro-reduction, with activities (TON, TOF) that can contend with the Re analogs.

Fei *et al.*[96] reported the post-synthetic metallation of a robust Zr(IV)-based metal-organic framework (MOF) with open bpy metal-chelating linkers to obtain isolated Mn(bpy)-$(CO)_3Br$ moieties in the MOF. Most significantly, in conjunction with $[Ru(dmb)_3]^{2+}$ as a redox photosensitizer and 1-benzyl-1,4-dihydronicotinamide (BNAH) as a propitiatory reducing agent, the resultant [UiO-67 Mn(bpy)$(CO)_3Br$] was realized to be immensely active and selective for the photocatalytic reduction of CO_2 to formate with a turnover number (TON) of 110 through 18 h of catalysis.

The suggested mechanism for the photocatalytic reaction is presented in this review (Figure 9). In these reactions, BNAH assists as the conciliatory reducing agent, reducing the excited Ru(II) photosensitizer and starting the photocatalytic reaction. There is an electron transmission from the reduced photosensitizer to the Mn catalyst, forming an absorbable Mn(0) during catalysis. The UiO-67[97-99] large pores, are copious to allow electron transfer amongst the Ru(II) photosensitizer and the Mn complex within the MOF, as the Ru(II) photosensitizer have the strength to allow the interior of UiO-67. TEOA plausibly improves the reaction by contributing a yielded proton and electron (i.e., a hydrogen atom) for the time of catalysis through a Hofmann-type degradation process (Figure 9)[100]. It is unaffirmed whether or not TEOA harmonizes the Mn center in the course of this process; nevertheless, co-joining

Eclética Química Journal, vol. 44, n. 1, 2019, 11-39
ISSN: 1678-4618
DOI: 10.26850/1678-4618eqj.v44.1.2019.p11-39

of CO_2 with the metal center is aided by TEOA, constituting an O-bound Re−OC(O)$OCH_2CH_2NR_2$ complex, this was made known in past studies with Re bipyridine catalysts[101]. Fei and co-workers propose TEOA giving one proton and one electron to the catalytic reaction, devising a Mn(I)−H complex. CO_2 can insert into the Mn−H bond, making a Mn(I)−OC(O)H complex. Formate (or formic acid after further protonation) can then be liberated from the Mn center renewing the starting Mn(I) complex. These conclusions are from the bulk of previously published work on photosensitized catalysis impelled by sacrificial reducing agents[102-107].

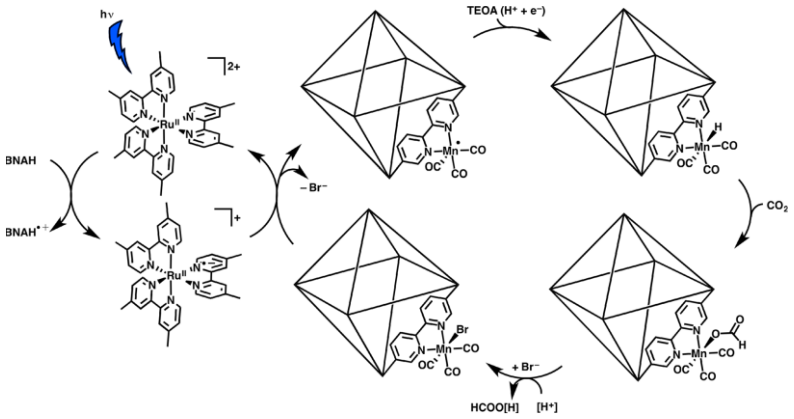

Figure 9. Suggested mechanism for the formation of formate from the photocatalytic reaction with UiO-67-Mn(bpy)$(CO)_3Br$[96]. *Reprinted with permission from Fei et al., Photocatalytic CO_2 Reduction to Formate Using a Mn(I) Molecular Catalyst in a Robust Metal–Organic Framework, Inorg. Chem. 54 (14) (2015) 6821-6828. Copyright (2015) American Chemical Society.*

According to Franco *et al.*[108], the first pure organometallic *fac*-[MnI$(CO)_3$(bis-MeNHC)Br] complex with the revolutionary operation for selective electrocatalytic CO_2-to-CO reduction, overreaching 100 turnovers CO with outstanding FE yields (ηCO~95%) in anhydrous CH_3CN. During similar state, CV was used determined maximum turnover frequency (TOF_{max}) of 2100 s^{-1}, thus, evidently greater than the values described for other Mn-based catalysts.

Experimental results account for the direct transformation of the [MnI$(CO)_3$(bis-MeNHC)Br] species (Figure 10), into five-coordinate [Mn$(CO)_3$(bis-MeNHC)]$^-$, the core product formed upon reduction. Importantly, the energy of the experimental CO stretching of [Mn$(CO)_3$(bis-MeNHC)]$^-$ show a powerfully localized negative charge over the Mn atom persistent with the bis-MeNHC ligand redox innocence. In fact, Kohn-Sham orbitals of [Mn$(CO)_3$(bis-MeNHC)]$^+$ to [Mn$(CO)_3$(bis-MeNHC)]• and [Mn$(CO)_3$(bis-MeNHC)]$^-$ indicate that the reduction occurs particularly over the metal center. The HOMO orbital geometry ([Mn$(CO)_3$(bis-MeNHC)]$^-$**)** is openly accessible to undertake a nucleophilic attack in contrast with [Mn$(CO)_3$(py-MeNHC)]$^-$. To summarize, the first family of organometallic NHC-based tricarbonyl Mn^I complexes active for electrocatalytic CO_2 reduction to CO was reported by Franco and co-workers[108]. Here, bis-MeNHC = methylene bis(N-methylimidazolium) ligand and py-MeNHC = N-methyl-N'-2-pyridilimidazolium ligand. Pyridine ring replacement with a NHC unit exceptionally influences the catalytic operation, to improve the TOF_{max} and selectivity for CO production of well-established C^N ligand-based Mn systems significantly. Additionally, the unique bis-NHC catalyst successfully and selectively adapts CO_2 to CO in an anhydrous aprotic organic solvent; differentially, the traditional bpy-based systems mainstream are unveiled to be inert without regard to definite proton source[109-114].

Eclética Química Journal, vol. 44, n. 1, 2019, 11-39
ISSN: 1678-4618
DOI: 10.26850/1678-4618eqj.v44.1.2019.p11-39

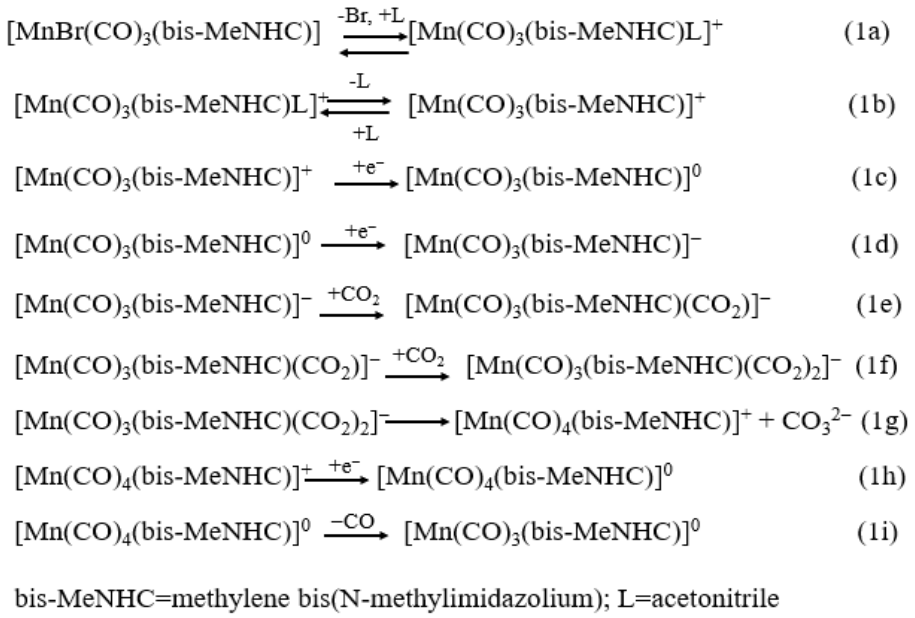

Figure 10. Proposed mechanism of CO_2 reduction to CO by *fac*-[MnI(CO)$_3$(bis-MeNHC)Br] complex [108].

Reuillard *et al.*[115] stated the assemblage of the complex [MnBr(2,2'-bipyridine)(CO)$_3$] attached to a carbon nanotube electrode over a pyrene unit. Molecular catalyst check allows electrocatalytic CO_2 reduction during entire aqueous conditions with a catalytic onset overpotential of η = 360 mV, and restrained potential electrolysis produced turnovers at η = 550 mV greater than 1000. The product selectivity is adjustable by catalyst amendment loading on the nanotube surface.

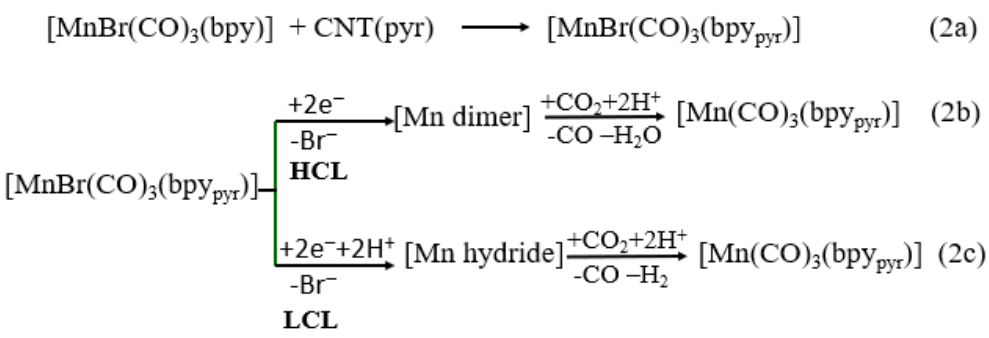

Figure 11. Proposed mechanism of *fac*-[MnBr(bpy$_{pyr}$)(CO)$_3$] immobilized on a CNT sidewall, concentration-dependent dimerization or Mn−H formation, and intermediate-dependent reduction of CO_2 to CO or HCOOH[115].

The complex [MnBr(bpy)(CO)$_3$] (bpy = 2,2'-bipyridine) is a noble metal-free model catalyst for CO_2 reduction consequent to the all-around and direct structure of the bpy ligand[30]. This catalyst displayed high activity (turnover frequency up = 480 s^{-1}) in MeCN, and its catalytic mechanism has been studied greatly by wavering the nature of the substituents on the bpy ligand[116-122]. The Mn catalyst was presently integrated onto CNTs utilizing Nafion[123], onto p-Si through polymerization[124], and onto TiO_2 via a phosphonate anchoring group[125]. The former system showed a

Eclética Química Journal, vol. 44, n. 1, 2019, 11-39
ISSN: 1678-4618
DOI: 10.26850/1678-4618eqj.v44.1.2019.p11-39

record turnover number (TON) for the Mn catalyst of 112 in MeCN[125]. The grafted Mn catalyst form a dimer on the electrode surface[125], as indicated by the UV−Vis spectra electrochemistry (SEC). It has also been enumerated in solution upon electrochemical reduction for this class of catalyst[126]. Despite the observations of these studies, yet, the reported activity is limited to organic solvents and low TONs (maximum of 101) in aqueous conditions[123]. The pyrene unit allowed stable immobilization onto CNTs. The compound, electrocatalytic activity, was the first study approaching the CO_2 reduction in the homogeneous organic solution (MeCN + 5% H_2O) and then in completely aqueous solutions after being heterogenized on the CNT surface. Using CPE and CV, the Mn catalyst modified electrodes were explored. The Mn complex surface loading was disclosed to have a unique effect on the selectivity toward CO or $HCOO^-$ production (Fig. 11). The different catalytic intermediates involved were investigated *in situ* through the application of transmission UV-VIS and surface-sensitive IR SEC in the impaired total reflection (ATR) mode. Selectivity toward either CO or $HCOO^-$ at various surface loadings, accurate formation assignment of one or the other catalytic intermediate is important[116, 122, 124].

2.3.4 Ni-based Molecular Catalyst

Nickel, a non-precious metal (group VIIIB), is considered the best possible alternative instead of palladium or platinum for molecular catalysts[127, 128] owing to its simply achievable oxidation states (e.g., Ni^0, Ni^I, Ni^{II}, Ni^{III}, and Ni^{IV}). The CO_2 reduction performed by nickel catalysts repeatedly required the Ni^{II} reduction to Ni^I, which is linked with the distortion of geometrical from a tetra-dentate, square planar coordination mode fitting for Ni^{II} to a tetrahedral one model for Ni^I [129-131]. Similarly, OER, the Ni^{II} oxidation to Ni^{III} typically allows the structural shift from a square planar to a tetragonal or octahedral geometry[132, 133]. Therefore, the rich redox properties connected with many coordination geometries concede the ligand logical form scaffolds to harmonize with nickel (II) centers, contributing to the nickel complexes with precise catalyst operations[133-138]. Moreover, nickel is an active center in natural enzymes, the well-known {NiFe} hydrogenases for the reversible conversion hydrogen, proton[139, 140], and the {NiFe} CO dehydrogenases (CODHs) for the reversible transformation between CO_2 and CO[141, 142]. These findings further compelled the scientist (mostly energy conversion catalysis), to develop molecular catalysts based on nickel complexes. In spite many insightful reviews on spotlighted earth-abundant metal complexes as catalysts for the HER[143-151], OER[152-154] and CO_2 reduction[155-162], however, details on the Ni-based molecular catalyst is yet to be available in the literature. More recently, Wang, Jia-Wei *et al.*[163] reported a systematical review on the recent developments in the utilization of nickel complexes as molecular catalysts for water splitting and CO_2 reduction. In summary, nickel cyclam complexes display high efficiency and selectivity. Nonetheless, other nickel-based catalysts display moderate activity, and selectivity, while the solvent used, is restricted to non-aqueous solvents.

Niu *et al.*[164] has designed and synthesized a spongy nickel-organic heterogeneous catalyst through the photochemical pathway. The catalyst possesses crystalline network architecture with a high imperfections concentration and active in CO_2 conversion to CO, with ~1.6×10^4 μmol h^{-1} g^{-1} production rate. During the reaction, no measurable H_2 is generated, resulting to approx. 100% selective CO production over the evolution of H_2 and the evolution of CO from these five Ni-organic catalysts in a photocatalytic 6 h response. The spongy Ni(TPA/TEG) (L) composite results to be the highest activity, and the CO amount is 95.2 mmol after a 2 h reaction, yielding to a CO production rate (15,866 μmol h^{-1} g^{-1}), that is many times greater than other samples. The total CO volume produced on the spongy Ni(TPA/TEG) catalyst in 6 h attains 136.9 μmol, giving a turnover of 11.5 for the 6 h reaction. By investigating the CO yield in 2 h on different amounts of Ni(TPA/TEG) catalyst, a roughly linear relationship was obtained between the number of CO evolved and the catalyst amount. However, kinetically, it was found that the CO production rate decrease is proportional to increase in the catalyst amount, where 1.0 mg of the Ni(TPA/TEG) catalyst results to CO production rate of ~26,620 μmol h^{-1} g^{-1} in a similar solution. Thus, implies that more electrons generated from the photosensitizer molecules may perhaps have been transferred to the active catalytic sites. Also, the reusability of the spongy Ni(TPA/TEG) catalyst upon each 2 h of photocatalysis have been tested, where the catalyst retained its activity and

Eclética Química Journal, vol. 44, n. 1, 2019, 11-39
ISSN: 1678-4618
DOI: 10.26850/1678-4618eqj.v44.1.2019.p11-39

selectivity after recycling. In addition, it also displays outstanding architectural stability with no apparent detectable structural change after 24 h of photocatalysis. For further confirmation of the origin of as-produced CO, isotopic $^{13}CO_2$ was used as feedstock gas for the photocatalytic reduction and the products were examined by gas chromatography-mass spectrometry (GC-MS). The study confirms that the detected CO originates from the CO_2 gas source; with the important signal at a mass/charge ratio (29) on the mass spectrum corresponding to ^{13}CO.

Consequence of the previous result, Niu and co-workers proposed the mechanism for the photocatalytic CO_2 reduction reactions on the spongy Ni(TPA/TEG) catalyst (Fig. 12). Based on visible light irradiation, the $[Ru(bpy)_3]^{2+}$ (photosensitizer) is excited and then reductively snuffed out by the sacrificial electron donor [TEOA, 65-167], resulting to the reduced species of $[Ru(bpy)_3]^{2+}$ (Fig. 12). Afterward, the $[Ru(bpy)_3]^{2+}$ reduced species could maybe transfer an electron to the spongy Ni(TPA/TEG) catalyst, which later engages in CO_2 molecules reducing fixed on the catalyst (Fig. 12). The yield tests of CO production in the solution with different Ni(TPA/TEG) amounts for 2 h, revealed that the CO production rate decreases with increase in the catalyst amount, indicating that the electron transfer from $[Ru(bpy)_3]^{2+}$ to the catalyst may be a rate-determining step for the CO_2 reduction reaction, however, limited diffusion scenario may have occurred in this heterogeneous catalytic system[168]. Thereafter, the derivative CO can be reduced to liquid fuels by means of proton-coupled multi-electron reaction processes (Fig. 12). In the electrolyte with a pH value of ~8, it was also suggested conversion pathways resulting to the HCOOH, CH_3COOH, and CH_3CH_2OH formation through proton-coupled one-, four-, and eight-electron steps, respectively.

In the mechanistic CH_3COOH formation route, CO is perpetually hydrated to $CHO \rightarrow CHOH \rightarrow CH_2OH \rightarrow CH_3OH$, which bonds with the adsorbed CO to form CH_3COOH. With a focus on the CH_3CH_2OH formation, the dehydroxylation of the as-formed CHO may possibly be a crucial rate-limiting step to produce additional C that can be protonated $CH \rightarrow CH_2 \rightarrow CH_3$[169], and the C–C coupling in the space separating CH_3 and multi protonated CO could result in the CH_3CH_2OH formation[170]. Frequently, the hydroxyl ions (OH^-) are obtained for the CHO hydroxylation at pH 13, which select the HCOOH formation. Whereas, the facilitated CHO hydroxylation may suppress the kinetics of the CO multi protonation and CHO dihydroxylation, yielding a lower amount of CH_3COOH and CH_3CH_2OH at pH 13. The CH_3OH appearance may present a weak C–C coupling in the space separating CH_3OH and CO at pH 13 (resulting to CH_3COOH at pH 8), hence, may be considered for the next CO_2/CO reduction catalyst design[171].

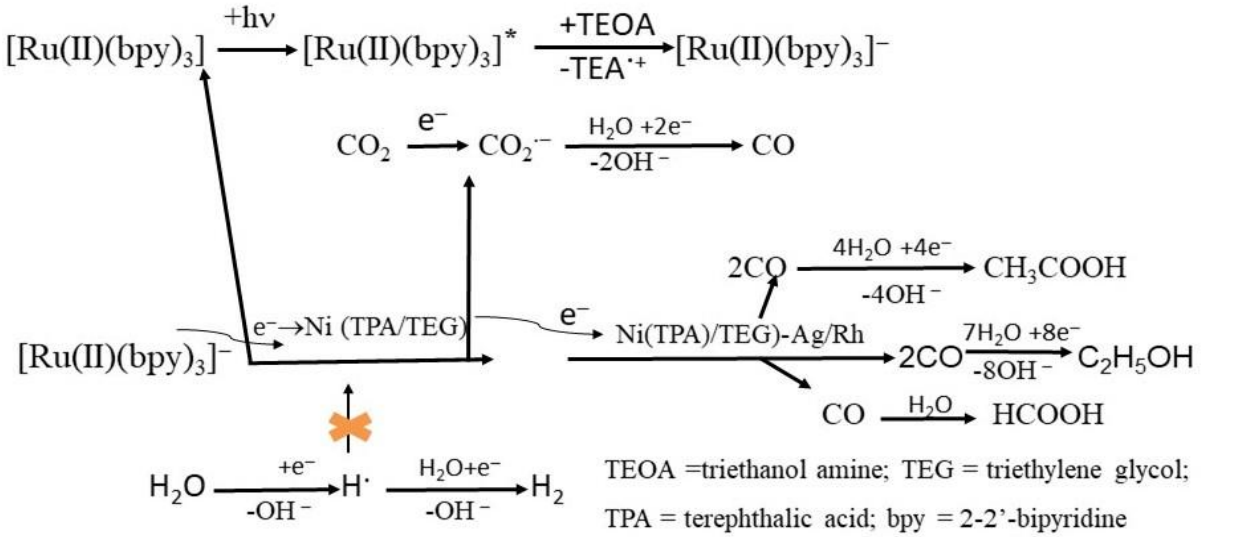

Figure 12. Proposed mechanisms for the photocatalytic reduction of CO_2 to CO and of CO to other liquid products. Visible light reduction of the photosensitizer $[Ru(bpy)_3]^{2+}$, which transfers an electron to the Ni(TPA/TEG) catalyst to convert CO_2 to CO and to Ni(TPA/TEG)-(Ag/Rh) catalysts for the generation of HCOOH, CH_3COOH, and CH_3CH_2OH from further reduction of CO[164].

Eclética Química Journal, vol. 44, n. 1, 2019, 11-39
ISSN: 1678-4618
DOI: 10.26850/1678-4618eqj.v44.1.2019.p11-39

Kuehnel *et al.*[172] investigated a series of self-assembled nickel terpyridine complexes as catalysts for the CO_2 reduction to CO in organic media. Immobilization on CdS quantum dots allows these catalysts to be functional in purely aqueous solution, and photo catalytically reduces CO_2 with > 90% selectivity in UV-filtered simulated solar light irradiation (AM 1.5G, 100 mW cm^{-2}, λ > 400 nm, pH 6.7). The QD-BF4 adjustments were performed in - situ through an additional stock solution of a self-assembled Ni complex to a suspension of QDs in TEOA aqueous solution (0.1 mol L^{-1}). This finally results into H_2O:CH3CN solution composition including 99:1 for $[Ni(terpy)_2]^{2+}$and $[Ni(terpyS)_2]^{2+}$, and 99.5:1 for $[Ni(terpyC)_2]^{2+}$ and $[Ni(terpyP)_2]^{2+}$. Catalyst attachment was affirmed by UV-vis spectroscopy with the anchoring group that involves dependent catalyst loading (Figure 13A). Considerably, the highest loading was accomplished with the thiol derivative, $[Ni(terpyS)_2]^{2+}$, while other anchors were measured with lower affinity (Figure 13B). The determination of main catalyst peaks in the UV-vis and ATR-IR spectra of $[Ni(terpyS)_2]^{2+}$–adjusted CdS QDs immobilized on a mesoporous SnO_2 electrode show that the catalyst maintained its intact chemical structure on the QD surface (Figures 13C). Cyclic voltammetry showed that the anchored catalyst retained its electrochemical response, additional supporting functional integrity on the QD surface (Figure 13D). Therefore, transmission electron microscopy unveiled that anchoring of the catalyst does not affect the particle morphology.

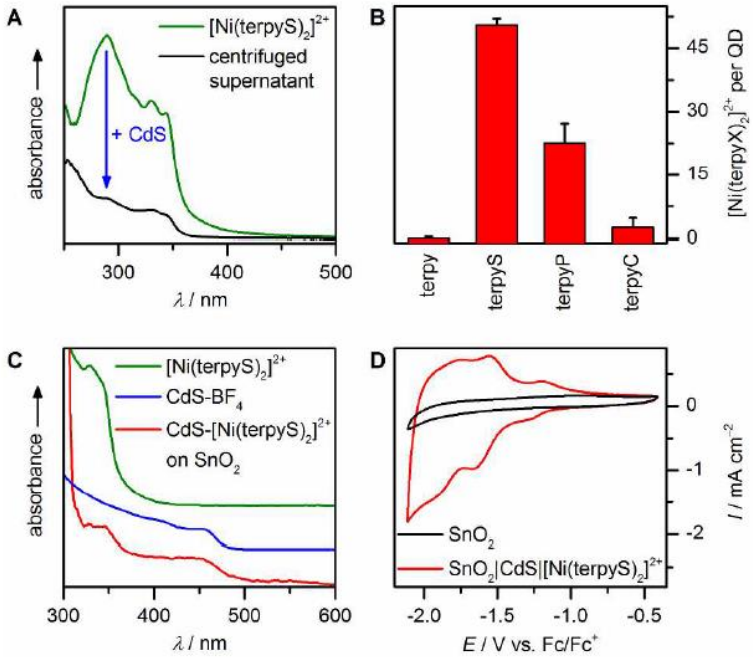

Figure 13. Hybrid photocatalyst assembly from CdS QDs and $[Ni(terpyX)_2]^{2+}$. A) Difference in UV-vis absorption of a $[Ni(terpyS)_2]^{2+}$ solution before and after stirring with CdS QDs; B) Adsorption efficiency of different $[Ni(terpyX)_2]^{2+}$ complexes; C) UV-vis spectra of CdS-$[Ni(terpyS)_2]^{2+}$ hybrid photocatalyst immobilized on a mesoporous SnO_2 electrode and comparison with CdS-BF4 and $[Ni(terpyS)_2]^{2+}$ in solution (spectra scaled and stacked for clarity); D) Cyclic voltammetry of CdS-$[Ni(terpyS)_2]^{2+}$ photocatalyst immobilized on a SnO_2 electrode[172]. *Reprinted with permission from Kuehnel et al., Selective Photocatalytic CO_2 Reduction in Water through Anchoring of a Molecular Ni Catalyst on CdS Nanocrystals, J. Am. Chem. Soc. 139 (21) (2017) 7217-7223. Copyright (2017) American Chemical Society.*

The photocatalytic activity of the congregated CdS-$[Ni(terpyX)_2]^{2+}$ hybrids were investigated in CO_2-saturated water under simulated solar light irradiation in the presence of TEOA (sacrificial electron donor). While the parent CdS-$[Ni(terpy)_2]^{2+}$ catalyst void of an anchoring group mainly yielded H_2 and only traces of CO, the functionalized derivatives displayed higher activities towards CO_2 reduction. $[Ni(terpyS)_2]^{2+}$ revealed both the highest CO_2 reduction activity, product selectivity series (92.2% after 4 h

Eclética Química Journal, vol. 44, n. 1, 2019, 11-39
ISSN: 1678-4618
DOI: 10.26850/1678-4618eqj.v44.1.2019.p11-39

compared to 10.2% and 3.9% for $[Ni(terpyP)_2]^{2+}$ and $[Ni(terpyC)_2]^{2+}$, respectively).

Surprisingly, the selectivity observed does not exhibit the electrocatalytic activity in the homogeneous phase, however, correlates with the adsorption efficiency of each complex to CdS. This behavior affirms that molecular catalyst interfacing with the nanoparticle is important to all-inclusive photocatalytic activity in aqueous solution. At the optimized state, about 20 Ni-based turnovers were obtained with CdS-$[Ni(terpyS)_2]^{2+}$ in 24 h visible light illumination. The CO selectivity continues to exist (> 90%) for the first 8 h prior to slowly decrease that mostly produce H_2 after 24 h. Ion-coupled plasma optical emission spectroscopy (ICP-OES) of QDs isolated from the reaction medium iterates the reducing selectivity co-occurs with a gradual $[Ni(terpyS)_2]^{2+}$ loss of the QD surface, differentially, the $CdSBF_4$ particles remain unchanged. UV-Vis spectra display a slight redshift of the first absorption, presenting limited particle aggregation with no significant photocorrosion. In addition, fresh catalyst after 20 h recovers the CO generation activity and subdue H_2 evolution, while the $Ni(BF4)_2$ addition only promotes H_2 evolution. Conversely, lessening the initial catalyst:QD ratio reduced the CO selectivity, moreover, it did not significantly affect the maximum TONCO (with respect to $[Ni(terpyS)_2]^{2+}$), where it can be inferred that a TONCO of ~20 represents the catalyst stability limit.

3. Conclusions and future perspectives

This general overview of the recent research on metal complex molecular catalysts for CO_2 reduction shows their contributions to the growing and dynamic field that gaining new insights into science at an ever-increasing rate. In order to increase metal complexes molecular catalysts application, it is imperative to overcome their poor stability which is a significant challenge. We suggest that one of the possible means to achieve this stability could be to ensure complexes heterogeneous, through their substrate's immobilization. Notwithstanding, the limited examples we have presented in this review, (e.g., porous structures, or covalent grafting on electrodes through ligand functionalization), suggest that the concept is realizable. Succinctly, the advancing knowledge acquired in several reduction mechanisms might give-way for more efficient selective and prolong metal complex molecular catalysts development. Additionally, most metal complexes molecular catalysts are light sensitive and suffer from photostability issues in any of these two ways; (i) by ligand photodissociation reactions and (ii) photoisomerization. This particular problem is an important obstacle towards the efficient metal complex photocatalysts for CO_2 reduction advancement. Unarguably, more improvements are still required, and other pathways for CO_2 catalytic reduction may perhaps offer ample fruitful opportunities.

5. Acknowledgments

This research did not receive any specific grant from funding agencies in the public, commercial, or not-for-profit organization. However, the authors are grateful to Mr. Abebe Reda of the University of Chinese Academy of Sciences, National Centre for Nanoscience and Technology, Beijing, China for his support and assistance.

6. References

[1] Qiao, J., Liu, Y., Hong, F., Zhang, J., A review of catalysts for the electroreduction of carbon dioxide to produce low-carbon fuels, Chem. Soc. Rev. 43 (2) (2014) 631-675. https://doi.org/10.1039/c3cs60323g.

[2] Liu, G., Hoivik, N., Wang, K., Jakobsen, H., Engineering TiO_2 nanomaterials for CO_2 conversion/solar fuels, Sol. Energ. Mat. Sol. C. (105) (2012) 53-68. https://doi.org/10.1016/j.solmat.2012.05.037.

[3] Costentin, C., Robert, M., Savéant, J.-M., Current Issues in Molecular Catalysis Illustrated by Iron Porphyrins as Catalysts of the CO_2-to-CO Electrochemical Conversion, Acc. Chem. Res. 48 (12) (2015) 2996-3006. https://doi.org/10.1021/acs.accounts.5b00262.

[4] Zhang, Y., Jacobs, G., Sparks, D. E., Dry, M. E., Davis, B. H., CO and CO_2 hydrogenation study on supported cobalt Fischer-Tropsch synthesis catalysts, Catal. Today 71 (3-4) (2002)

Eclética Química Journal, vol. 44, n. 1, 2019, 11-39
ISSN: 1678-4618
DOI: 10.26850/1678-4618eqj.v44.1.2019.p11-39

411-418. https://doi.org/10.1016/S0920-5861(01)00468-0.

[5] Lu, Q., Rosen, J., Zhou, Y., Hutchings, G. S., Kimmel, Y. C., Chen, J. G., Jiao, F., A selective and efficient electrocatalyst for carbon dioxide reduction, A Nat. Commun. (2014) 5. https://doi.org/3242.10.1038/ncomms4242.

[6] Nie, X., Esopi, M. R., Janik, M. J., Asthagiri, A., Selectivity of CO_2 reduction on copper electrodes: the role of the kinetics of elementary steps, Angew. Chem. 52 (9) (2013) 2459-2462. https://doi.org/10.1002/anie.201208320.

[7] Lu, Q., Rosen, J., Jiao, F., Nanostructured metallic electrocatalysts for carbon dioxide reduction, Chem. Cat. Chem. 7 (1) (2015) 38-47. https://doi.org/10.1002/cctc.201402669.

[8] Hori, Y., Electrochemical CO_2 Reduction on Metal Electrodes. In: Modern Electrochemistry, vol. 42, Vayenas, C. G., White, R. E., Gamboa-Aldeco, M. E., Eds.; Springer New York: New York, NY, 2008; pp 89-189.

[9] Liu, X., Ye, L., Liu, S., Li, Y., Ji, X., Photocatalytic Reduction of CO_2 by ZnO Micro/nanomaterials with Different Morphologies and Ratios of {0001} Facets, Scientific Reports volume 6, Article number: 38474 (2016). https://doi.org/10.1038/srep38474.

[10] Chen, Y., Kanan, M. W. J., Tin oxide dependence of the CO_2 reduction efficiency on tin electrodes and enhanced activity for tin/tin oxide thin-film catalysts, J. Am. Chem. Soc. 134 (4) (2012) 1986-1989. https://doi.org/10.1021/ja2108799.

[11] Asadi, M., Kumar, B., Behranginia, A., Rosen, B. A., Baskin, A., Repnin, N., Pisasale, D., Phillips, P., Zhu, W., Haasch, R., Klie, R. F., Král, P., Abiade, J., Salehi-Khojin, A., Robust carbon dioxide reduction on molybdenum disulphide edges, Nat. Commun. 5 (2014) Article number: 4470. https://doi.org/10.1038/ncomms5470.

[12] Asadi, M., Kim, K., Liu, C., Addepalli, A. V., Abbasi, P., Yasaei, P., Phillips, P., Behranginia, A., Cerrato, J. M., Haasch, R., Zapol, P., Kumar, B., Klie, R. F., Abiade, J., Curtiss, L. A., Salehi-Khojin, A., Nanostructured transition metal dichalcogenide electrocatalysts for CO_2 reduction in ionic liquid, Science 353 (6298) (2016) 467-470. https://doi.org/10.1126/science.aaf4767.

[13] Collin, J. P., Sauvage, J. P., Electrochemical reduction of carbon dioxide mediated by molecular catalysts, Coord. Chem. Rev. 93 (2) (1989) 245-268. https://doi.org/10.1016/0010-8545(89)80018-9.

[14] Savéant, J.-M., Molecular catalysis of electrochemical reactions. Mechanistic aspects, Chem. Rev. 108 (7) (2008) 2348-2378. https://doi.org/10.1021/cr068079z.

[15] Takeda, H., Cometto, C., Ishitani, O., Robert, M., Electrons, photons, protons and earth-abundant metal complexes for molecular catalysis of CO_2 reduction, ACS Catal. 7 (1) (2017) 70-88. https://doi.org/10.1021/acscatal.6b02181.

[16] Li, L., Yan, J., Wang, T., Zhao, Z. J., Zhang, J., Gong, J., Guan, N., Sub-10 nm rutile titanium dioxide nanoparticles for efficient visible-light-driven photocatalytic hydrogen production, Nat. Commun. 6 article number: 5881 (2015). https://doi.org/10.1038/ncomms6881.

[17] Wang, J. C., Zhang, L., Fang, W. X., Ren, J., Li, Y. Y., Yao, H. C., Wang, J. S., Li, Z. J., Enhanced photoreduction CO_2 activity over direct z-scheme α-Fe_2O_3/Cu_2O heterostructures under visible light irradiation, ACS Appl. Mater. Interfaces 7 (16) (2015) 8631-8639. https://doi.org/10.1021/acsami.5b00822.

[18] Kudo, A., Miseki, Y., Heterogeneous photocatalyst materials for water splitting, Chem.

Eclética Química Journal, vol. 44, n. 1, 2019, 11-39
ISSN: 1678-4618
DOI: 10.26850/1678-4618eqj.v44.1.2019.p11-39

Soc. Rev. 38 (1) (2009) 253-278. https://doi.org/10.1039/b800489g.

[19] Hisatomi, T., Kubota, J., Domen, K., Recent advances in semiconductors for photocatalytic and photoelectrochemical water splitting, Chem. Soc. Rev. 43 (2014) 7520-7535. https://doi.org/10.1039/C3CS60378D.

[20] Ma, Y., Wang, X., Jia, Y., Chen, X., Han, H., Li, C., Titanium dioxide-based nanomaterials for photocatalytic fuel generations, Chem. Rev. 114 (19) (2014) 9987-10043. https://doi.org/10.1021/cr500008u.

[21] Kang, D., Kim, T. W., Kubota, S. R., Cardiel, A. C., Cha, H. G., Choi, K. S., Electrochemical synthesis of photoelectrodes and catalysts for use in solar water splitting, Chem. Rev. 115 (23) (2015) 12839-12887. https://doi.org/10.1021/acs.chemrev.5b00498.

[22] Tong, H., Ouyang, S., Bi, Y., Umezawa, N., Oshikiri, M., Ye, J., Nano-photocatalytic materials: possibilities and challenges, Adv. Mater. 24 (2) (2012) 229-251. https://doi.org/10.1002/adma.201102752.

[23] Ran, J., Zhang, J., Yu, J., Jaroniec, M., Qiao, S. Z., Earth-abundant cocatalysts for semiconductor-based photocatalytic water splitting, Chem. Soc. Rev. 43 (22) (2014) 7787-7812. https://doi.org/10.1021/jacs.5b04186.

[24] Chang, X., Wang, T., Zhang, P., Zhang, J., Li, A., Gong, J., Enhanced surface reaction kinetics and charge separation of p–n heterojunction Co_3O_4/$BiVO_4$ photoanodes, J. Am. Chem. Soc. 137 (26) (2015) 8356-8359. https://doi.org/10.1021/jacs.5b04186.

[25] England, J., Bill, E., Weyhermüller, T., Neese, F., Atanasov, M., Wieghardt, K., Molecular and electronic structures of homoleptic six-coordinate cobalt(I) complexes of 2,2':6',2''-terpyridine, 2,2'-bipyridine, and 1,10-phenanthroline. An experimental and computational study, Inorg. Chem. 54 (24) (2015) 12002-12018. https://doi.org/10.1021/acs.inorgchem.5b02415.

[26] Wang, M., Weyhermüller, T., Bill, E., Ye, S., Wieghardt, K., Structural and spectroscopic characterization of rhenium complexes containing neutral, monoanionic, and dianionic ligands of 2, 2′-bipyridines and 2,2′:6,2″-Terpyridines: An Experimental and Density Functional Theory (DFT)-Computational Study, Inorg. Chem. 55 (10) (2016) 5019-5036. https://doi.org/10.1021/acs.inorgchem.6b00609.

[27] Wang, M., England, J., Weyhermu, T., Wieghardt, K., Molecular and electronic structures of the members of the electron transfer series $[Mn(bpy)_3]^n$ (n = 2+, 1+, 0, 1−) and $[Mn(tpy)_2]^m$ (m = 4+, 3+, 2+, 1+, 0). An experimental and density functional theory study, Inorg. Chem. 53 (4) (2014) 2276-2287. https://doi.org/10.1021/ic4029854.

[28] Scarborough, C. C., Lancaster, K. M., DeBeer, S., Weyhermueller, T., Sproules, S., Wieghardt, K., Experimental fingerprints for redox-active terpyridine in $[Cr(tpy)_2](PF_6)_n$ (n = 3–0), and the remarkable electronic structure of $[Cr(tpy)_2]^{1-}$, Inorg. Chem. 51 (6) (2012) 3718-3732. https://doi.org/10.1021/ic2027219.

[29] Paddon, C. A., Atobe, M., Fuchigami, T., He, P., Watts, P., Haswell, S. J., Pritchard, G. J., Bull, S. D., Marken, F. J., Towards paired and coupled electrode reactions for clean organic microreactor electrosyntheses, Appl. Electrochem. 36 (6) (2006) 617-634. https://doi.org/10.1007/s10800-006-9122-2.

[30] Pütter, H., Organic Electrochemistry, 4th ed., Lund, H., Hammerich, O., Eds., Marcel Dekker: New York, 2001; 1259-1308.

[31] Frontana-Uribe, B. A., Little, R. D., Ibanez, J. G., Palma, A., Vasquez-Medrano, R., Organic electrosynthesis: a promising green methodology in organic chemistry, Green Chem.

12 (2010) 2099-2119. https://doi.org/10.1039/C0GC00382D.

[32] Tatin, A., Comminges, C., Kokoh, B., Costentin, C., Robert, M., Savéant, J.-M., Efficient electrolyzer for CO_2 splitting in neutral water using earth-abundant materials, Proc. Natl. Acad. Sci. U. S. A. 113 (20) (2016) 5526-5529. https://doi.org/10.1073/pnas.1604628113.

[33] Parajuli, R., Gerken, J. B., Keyshar, K., Sullivan, I., Sivasankar, N., Teamey, K., Stahl, S. S., Cole, E. B, Integration of anodic and cathodic catalysts of earth-abundant materials for efficient, scalable CO_2 reduction, Top. Catal. 58 (1) (2015) 57-66. https://doi.org/10.1007/s11244-014-0345-x.

[34] Kim, B., Ma, S., Molly Jhong, H.-R., Kenis, P. J. A., Influence of dilute feed and pH on electrochemical reduction of CO_2 to CO on Ag in a continuous flow electrolyzer, Electrochim. Acta 166 (2015) 271-276. https://doi.org/10.1016/j.electacta.2015.03.064.

[35] Luc, W., Rosen, J., Jiao, F., An Ir-based anode for a practical CO_2 electrolyzer, Catal. Today 288 (2016) 79-84. https://doi.org/10.1016/j.cattod.2016.06.011.

[36] Sebastián, D., Palella, A., Baglio, V., Spadaro, L., Siracusano, S., Negro, P., Niccoli, F., Arico, A. S., CO_2 reduction to alcohols in a polymer electrolyte membrane co-electrolysis cell operating at low potentials, Electrochim. Acta 241 (2017) 28-40. https://doi.org/10.1016/j.electacta.2017.04.119.

[37] Benson, E. E., Kubiak, C. P., Sathrum, A. J., Smieja, J. M., Electrocatalytic and homogeneous approaches to conversion of CO_2 to liquid fuels, Chem. Soc. Rev. 38 (1) (2009) 89-99. https://doi.org/10.1039/b804323j.

[38] Llorente, M. J., Nguyen, B. H., Kubiak, C. P., Moeller, K. D. J., Paired electrolysis in the simultaneous production of synthetic intermediates and substrates, J. Am. Chem. Soc. 138 (46) (2016) 15110-15113. https://doi.org/10.1021/jacs.6b08667.

[39] Mascetti, J., Carbon dioxide as a chemical feedstock paired electrolysis in the simultaneous production of synthetic intermediates and substrates. In: Carbon dioxide as a chemical feedstock, Aresta, M., Ed., Wiley-VCH, Weinheim 2010, chapter: 4th, pp.55-88.

[40] Gibson, D. H., Carbon dioxide coordination chemistry: metal complexes and surface-bound species. What relationships?, Coord. Chem. Rev. 185 (1) (1999) 335-355. https://doi.org/10.1016/S0010-8545(99)00021-1.

[41] Goedecke, C., Hillebrecht, P., Uhlemann, T., Haunschild, R., Frenking, G., The Dewar–Chatt–Duncanson model reversed — Bonding analysis of group-10 complexes $[(PMe_3)_2M–EX_3]$ (M = Ni, Pd, Pt; E = B, Al, Ga, In, Tl; X = H, F, Cl, Br, I), Can. J. Chem. 87 (10) (2009) 1470-1479. https://doi.org/10.1139/V09-099.

[42] Francke, R., Schille, B., Roemelt, M., Homogeneously catalyzed electroreduction of carbon dioxide-methods, mechanisms, and catalysts, Chem. Rev. 118 (9) (2018) 4631-4701. https://doi.org/10.1021/acs.chemrev.7b00459.

[43] Eisenberg, R., Hendrickson, D. E., The binding and activation of carbon monoxide, carbon dioxide, and nitric oxide and their homogeneously catalyzed reactions, Adv. Catal. 28 (14) (1979) 79-172. https://doi.org/10.1016/S0360-0564(08)60134-0.

[44] (a) Herskovitz, T., Carbon dioxide coordination chemistry. 3. Adducts of carbon dioxide with iridium (I) complexes, J. Am. Chem. Soc. 99 (7) (1977) 2391-2392. https://doi.org/10.1021/ja00449a087; (b) Calabrese, J. C., Herskovitz, T., Kinney, J. B., Carbon dioxide coordination chemistry. 5. The preparation ans structure of the rhodium complex Rh(□1-CO2)(Cl)(diars)2, J. Am. Chem. Soc. 105

Eclética Química Journal, vol. 44, n. 1, 2019, 11-39
ISSN: 1678-4618
DOI: 10.26850/1678-4618eqj.v44.1.2019.p11-39

(1983) 5914-5915. https://doi.org/10.1021/ja00356a033.

[45] Aresta, M., Nobile, C. F., Albano, V. G., Forni, E., Manassero, M., New nickel-carbon dioxide complex: synthesis, properties, and crystallographic characterization of (carbon dioxide)-bis(tricyclohexylphosphine)nickel, J. Chem. Soc. Chem. Commun. 15 (1975) 636-637. https://doi.org/10.1039/C39750000636.

[46] Karsch, H. H., Funktionelle Trimethylphosphinderivate, III. Ambivalentes Verhalten von Tetrakis (trimethylphosphin) eisen: Reaktion mit CO_2, Chem. Ber. 110 (6) (1977) 2213-2221. https://doi.org/10.1002/cber.19771100619.

[47] Komiya, S., Akita, M., Kasuga¸ N., Hirano¸ M., Fukuoka¸ A., Synthesis, structure and reactions of a carbon dioxide complex of iron (0) containing 1,2-bis(diethylphosphino)ethane ligands, J. Chem. Soc. Chem. Commun. 9 (1994) 1115-1116. https://doi.org/10.1039/C39940001115.

[48] Lewis, N. S., Nocera, D. G., Powering the planet: chemical challenges in solar energy utilization, Proc. Natl. Acad. Sci. 103 (43) (2006) 15729-15735. https://doi.org/10.1073/pnas.0603395103.

[49] a) Qiao, J., Liu, Y., Hong, F., Zhang, J., A review of catalysts for the electroreduction of carbon dioxide to produce low-carbon fuels, Chem. Soc. Rev., 43 (2014) 631-675. https://doi.org/10.1039/c3cs60323g; b) Portenkirchner, E., Oppelt, K., Egbe, D. A. M., Knör G., Sariçiftçi, N. S., Electro-and photo-chemistry of rhenium and rhodium complexes for carbon dioxide and proton reduction: a mini review, Nanomaterials and Energy 2 (2013) 134-147. https://doi.org/10.1680/nme.13.00004; c) Lim, R. J., Xie, M., Sk, M. A., Lee, J.-M., Fisher, A., Wang, X., Lim, K. H., A review on the electrochemical reduction of CO_2 in fuel cells, metal electrodes and molecular catalysts, Catal. Today 233 (15) (2014) 169-180. https://doi.org/10.1016/j.cattod.2013.11.037.

[50] a) Lin, S., Diercks, C. S., Zhang, Y.-B., Kornienko, N., Nichols, E. M., Zhao, Y., Paris, A. R., Kim, D., Yang, P., Yaghi, O. M., Chang, C. J., Covalent organic frameworks comprising cobalt porphyrins for catalytic CO_2 reduction in water, Science 349 (6253) (2015) 1208-1213. https://doi.org/10.1126/science.aac8343; b) Matlachowski, C., Braun, B., Tschierlei, S., Schwalbe, M., Photochemical CO_2 Reduction Catalyzed by Phenanthroline Extended Tetramesityl Porphyrin Complexes Linked with a Rhenium(I) Tricarbonyl Unit, Inorg. Chem. 54 (21) (2015) 10351-10360. https://doi.org/10.1021/acs.inorgchem.5b01717; c) Hod, I., Sampson, M. D., Deria, P., Kubiak, C. P., Farha, O. K., Hupp, J. T., Fe-Porphyrin-Based Metal–Organic Framework Films as High-Surface Concentration, Heterogeneous Catalysts for Electrochemical Reduction of CO_2, ACS Catal. 5 (11) (2015) 6302-6309. DOI: 10.1021/acscatal.5b01767; d) Costentin, C., Passard, G., Robert, M., Savéant, J.-M., Ultraefficient homogeneous catalyst for the CO_2-to-CO electrochemical conversion, Proc. Natl. Acad. Sci. 111 (42) (2014) 14990-14994. https://doi.org/10.1073/pnas.1416697111.

[51] [51] Taheri, A., Thompson, E. J., Fettinger, J. C., Berben, L. A., An iron electrocatalyst for selective reduction of CO_2 to formate in water: including thermochemical insights, ACS Catal. 5 (12) (2015) 7140-7151. https://doi.org/10.1021/acscatal.5b01708.

[52] Ambre, R. B., Daniel, Q., Fan, T., Chen, H., Zhang, B., Wang, L., Ahlquist, M. S. G., Duan, L., Sun, L., Molecular engineering for efficient and selective iron porphyrin catalysts for electrochemical reduction of CO_2 to CO, Chem. Commun. 52 (2016) 14478-14481. https://doi.org/10.1039/c6cc08099e.

[53] Bhugun, I., Lexa, D., Savéant, J.-M., Catalysis of the electrochemical reduction of

Eclética Química Journal, vol. 44, n. 1, 2019, 11-39
ISSN: 1678-4618
DOI: 10.26850/1678-4618eqj.v44.1.2019.p11-39

carbon dioxide by iron (0) porphyrins: Synergystic effect of weak Brönsted acids, J. Am. Chem. Soc. 118 (7) (1996) 1769-1776. https://doi.org/10.1021/ja9534462.

[54] Bhugun, I., Lexa, D., Savéant, J.-M., Ultraefficient selective homogeneous catalysis of the electrochemical reduction of carbon dioxide by an iron (0) porphyrin associated with a weak Broensted acid cocatalyst, J. Am. Chem. Soc. 116 (11) (1994) 5015-5016. https://doi.org/10.1021/ja00090a068.

[55] Costentin, C., Drouet, S., Passard, G., Robert, M., Savéant, J.-M., Proton-coupled electron transfer cleavage of heavy-atom bonds in electrocatalytic processes. Cleavage of a C–O bond in the catalyzed electrochemical reduction of CO_2, J. Am. Chem. Soc. 135 (24) (2013) 9023-9031. https://doi.org/10.1021/ja4030148.

[56] Rao, H., Schmidt, L. C., Bonin, J., Robert, M., Visible-light-driven methane formation from CO_2 with a molecular iron catalyst, Nature 548 (2017) 74-77. https://doi.org/10.1038/nature23016.

[57] Costentin, C., Robert, M., Savéant, J.-M., Tatin, A., Efficient and selective molecular catalyst for the CO_2-to-CO electrochemical conversion in water, Proc. Natl Acad. Sci. USA 112 (2015) 6882-6886. https://doi.org/10.1073/pnas.1507063112.

[58] Azcarate, I., Costentin, C., Robert, M., Savéant, J.-M., Through-Space Charge Interaction Substituent Effects in Molecular Catalysis Leading to the Design of the Most Efficient Catalyst of CO_2-to-CO Electrochemical Conversion, J. Am. Chem. Soc. 138 (51) (2016) 16639-16644. https://doi.org/10.1021/jacs.6b07014.

[59] Bonin, J., Maurin, A., Robert, M., Molecular catalysis of the electrochemical and photochemical reduction of CO_2 with Fe and Co metal based complexes. Recent advances, Coord. Chem. Rev. 334 (2017) 184-198. https://doi.org/10.1016/j.ccr.2016.09.005.

[60] Davies, S. G., Hibberd, J., Simpson, S. J., Disproportionation of the iron carbonyl hydride $(\eta^5\text{-}C_5H_5)Fe(CO)H(Ph_2PCH_2CH_2PPh_2)$ to the iron methyl $(\eta^5\text{-}C_5H_5)FePh_2PCH_2CH_2PPh_2)Me.$, J. Chem. Soc. Chem. Commun. (24) (1982) 1404-1405. https://doi.org/10.1039/C39820001404.

[61] Appel, A. M., Bercaw, J. E., Bocarsly, A. B., Dobbek, H., DuBois, D. L., Dupuis, M., Ferry, J. G., Fujita, E., Hille, R., Kenis, P. J. A., Kerfeld, C. A., Morris, R. H., Peden, C. H. F., Portis, A. R., Ragsdale, S. W., Rauchfuss, T. B., Reek, J. N. H., Seefeldt, L. C., Thauer, R. K., Waldrop, G. L., Frontiers, Opportunities, and Challenges in Biochemical and Chemical Catalysis of CO2 Fixation, Chem. Rev. 113 (8) (2013) 6621-6658. https://doi.org/10.1021/cr300463y.

[62] Pan, F., Zhang, H., Liu, K., Cullen, D., More, K., Wang, M., Feng, Z., Wang, G., Wu, G., Li, Y., Unveiling Active Sites of CO_2 Reduction on Nitrogen-Coordinated and Atomically Dispersed Iron and Cobalt Catalysts, ACS Catal. 8 (4) (2018) 3116-3122. https://doi.org/10.1021/acscatal.8b00398.

[63] Nichols, E. M., Derrick, J. S., Nistanaki, S. K., Smith, P. T., Chang, C. J., Positional effects of second-sphere amide pendants on electrochemical CO_2 reduction catalyzed by iron porphyrins, Chem. Sci. 9 (11) (2018) 2952-2960. https://doi.org/10.1039/c7sc04682k.

[64] Costentin, C., Drouet, S., Robert, M., Savéant, J.-M., Turnover numbers, turnover frequencies, and overpotential in molecular catalysis of electrochemical reactions. Cyclic voltammetry and preparative-scale electrolysis, J. Am. Chem. Soc. 134 (27) (2012) 11235-11242. https://doi.org/10.1021/ja303560c.

[65] Azcarate, I., Costentin, C., Robert, M., Savéant, J.-M., Dissection of Electronic Substituent Effects in Multielectron–Multistep Molecular Catalysis. Electrochemical CO_2-to-CO Conversion Catalyzed by Iron Porphyrins, J. Phys.

Eclética Química Journal, vol. 44, n. 1, 2019, 11-39
ISSN: 1678-4618
DOI: 10.26850/1678-4618eqj.v44.1.2019.p11-39

Chem. C 120 (51) (2016) 28951-28960. https://doi.org/10.1021/acs.jpcc.6b09947.

[66] Pegis, M. L., McKeown, B. A., Kumar, N., Lang, K., Wasylenko, D. J., Zhang, X. P., Raugei, S., Mayer, J. M., Homogenous Electrocatalytic Oxygen Reduction Rates Correlate with Reaction Overpotential in Acidic Organic Solutions, ACS Cent. Sci. 2 (11) (2016) 850-856. https://doi.org/10.1021/acscentsci.6b00261.

[67] Azcarate, I., Costentin, C., Robert, M., Savéant, J.-M., Through-Space Charge Interaction Substituent Effects in Molecular Catalysis Leading to the Design of the Most Efficient Catalyst of CO_2-to-CO Electrochemical, J. Am. Chem. Soc. 138 (51) (2016) 16639-16644. https://doi.org/10.1021/jacs.6b07014.

[68] Specklin, D., Fliedel, C., Gourlaouen, C., Bruyere, J.-C., Avilés, T., Boudon, C., Ruhlmann, L., Dagorne, S., N-Heterocyclic Carbene Based Tri-organyl-Zn–Alkyl Cations: Synthesis, Structures, and Use in CO_2 Functionalization, Chem. Eur. J. 23 (23) 5509-5519. https://doi.org/10.1002/chem.201605907.

[69] Sattler, W., Parkin, G., Zinc catalysts for on-demand hydrogen generation and carbon dioxide functionalization, J. Am. Chem. Soc. 134 (42) (2012) 17462-17465. https://doi.org/10.1021/ja308500s.

[70] Specklin, D., Hild, F., Fliedel, C., Gourlaouen, C., Veiros, L. F., Dagorne, S., Accessing Two-Coordinate Zn^{II} Organocations by NHC Coordination: Synthesis, Structure, and Use as π-Lewis Acids in Alkene, Alkyne, and CO_2 Hydrosilylation, Chem. Eur. J 23 (63) (2017) 15908-15912. https://doi.org/10.1002/chem.201704382.

[71] Rauch, M., Parkin, G., Zinc and Magnesium Catalysts for the Hydrosilylation of Carbon Dioxide, J. Am. Chem. Soc. 139 (50) (2017) 18162-18165. https://doi.org/10.1021/jacs.7b10776.

[72] Rit, A., Zanardi, A., Spaniol, T. P., Maron, L., Okuda, J., A Cationic Zinc Hydride Cluster Stabilized by an N-Heterocyclic Carbene: Synthesis, Reactivity, and Hydrosilylation Catalysis, Angew. Chem. Int. Ed. 53 (48) (2014) 13273-13277. https://doi.org/10.1002/anie.201408346.

[73] Donovan, E. S., Barry, B. M., Larsen, C. A., Wirtz, M. N., Geiger, W. E., Kemp, R. A., Facilitated carbon dioxide reduction using a Zn(II) complex, Chem. Commun. 52 (8) (2016) 1685-1688. https://doi.org/10.1039/C5CC07318A.

[74] Hammouche, M., Lexa, D., Momenteau, M., Savéant, J.-M., Chemical catalysis of electrochemical reactions. Homogeneous catalysis of the electrochemical reduction of carbon dioxide by iron("0") porphyrins. Role of the addition of magnesium cations, J. Am. Chem. Soc. 113 (22) (1991) 8455-8466. https://doi.org/10.1021/ja00022a038.

[75] Wu, Y., Jiang, J., Weng, Z., Wang, M., Broere, D. L. J., Zhong, Y, Brudvig, G. W., Feng, Z., Wang, H., Electroreduction of CO_2 Catalyzed by a Heterogenized Zn-Porphyrin Complex with a Redox-Innocent Metal Center, ACS Central Science 3 (8) (2017) 847-852. https://doi.org/10.1021/acscentsci.7b00160.

[76] Won, D. H., Shin, H., Koh, J., Chung, J., Lee, H. S., Kim, H., Woo, S. I., Highly Efficient, Selective, and Stable CO_2 Electroreduction on a Hexagonal Zn Catalyst, Angew. Chem., Int. Ed. 55 (32) (2016) 9297-9300. https://doi.org/10.1002/anie.201602888.

[77] Hori, Y., Kikuchi, K., Suzuki, S., Production of CO and CH_4 in electrochemical reduction of CO_2 at metal electrodes in aqueous hydrogencarbonate solution, Chem. Lett. 14 (11) (1985) 1695-1698. https://doi.org/10.1246/cl.1985.1695.

[78] Hori, Y., Wakebe, H., Tsukamoto, T., Koga, O., Electrocatalytic process of CO selectivity in

Eclética Química Journal, vol. 44, n. 1, 2019, 11-39
ISSN: 1678-4618
DOI: 10.26850/1678-4618eqj.v44.1.2019.p11-39

electrochemical reduction of CO_2 at metal electrodes in aqueous media, Electrochim. Acta 39 (11-12) (1994) 1833-1839. https://doi.org/10.1016/0013-4686(94)85172-7.

[79] Wei, C., Feng, Z., Baisariyev, M., Yu, L., Zeng, L., Wu, T., Zhao, H., Huang, Y., Bedzyk, M. J., Sritharan, T., Xu, Z., Multifunctional mixed valence N-doped CNT@MFe_2O_4 hybrid nanomaterials: from engineered one-pot coprecipitation to application in energy storage paper supercapacitors, J. Chem. Mater. 28 (12) (2016) 4129-4133. https://doi.org/10.1039/C8NR03533D.

[80] Lin, S., Diercks, C. S., Zhang, Y.-B., Kornienko, N., Nichols, E. M., Zhao, Y., Paris, A. R., Kim, D., Yang, P., Yaghi, O. M., Chang, C. J., Covalent organic frameworks comprising cobalt porphyrins for catalytic CO_2 reduction in water, Science 349 (6253) (2015) 1208-1213. https://doi.org/10.1126/science.aac8343.

[81] Closs, G. L., Closs, L. E., Negative ions of porphin metal complexes, J. Am. Chem. Soc. 85 (6) (1963) 818-819. https://doi.org/10.1021/ja00889a038.

[82] Balducci, G., Chottard, G., Gueutin, C., Lexa, D., Savéant, J.-M., Electrochemistry of iron(I) porphyrins in the presence of carbon monoxide. Comparison with zinc porphyrins, Inorg. Chem. 33 (9) (1994) 1972-1978. https://doi.org/10.1021/ic00087a038.

[83] Lanese, J. G., Wilson, G. S J., Electrochemical studies of zinc tetraphenylporphin, Electrochem. Soc. 119 (8) (1972) 1039-1043. https://doi.org/10.1149/1.2404391.

[84] Lin, C.-L., Fang, M.-Y., Cheng, S.-H J., Substituent and axial ligand effects on the electrochemistry of zinc porphyrins, Electroanal. Chem. 531 (2) (2002) 155-162. https://doi.org/10.1016/S0022-0728(02)01056-2.

[85] Connelly, N. G., Geiger, W. E., Chemical redox agents for organometallic chemistry, Chem. Rev. 96 (2) (1996) 877-910. https://doi.org/10.1021/cr940053x.

[86] Parkhots, O. P., Ivashin, N. V., Study of the structure and spectral properties of radical anions of Zn complexes of porphyrins by the method of density functional theory, Opt. Spectrosc. 106 (2) (2009) 204-212 https://doi.org/10.1134/S0030400X0902009X.

[87] Wang, Y., Hou, P., Wang, Z., Kang, P., Zinc Imidazolate Metal–Organic Frameworks (ZIF-8) for Electrochemical Reduction of CO_2 to CO, ChemPhysChem. 18 (2017) 3142-3147. https://doi.org/10.1002/cphc.201700716.

[88] Kemmitt, R. D. W., Peacock, R. D., The Chemistry of Manganese, Technetium and Rhenium, Pergamon Press, 1973.

[89] Valyaev, D. A., Lavigne, G., Lugan, N., Manganese organometallic compounds in homogeneous catalysis: past, present, and prospects, Coord. Chem. Rev. 308 (2016) 191-235. https://doi.org/10.1016/j.ccr.2015.06.015.

[90] Sinopoli, A., La Porte, N. T., Martinez, J. F., Wasielewski, M. R., Sohail, M., Manganese carbonyl complexes for CO_2 reduction, Coord. Chem. Rev. 365 (2018) 60-74. https://doi.org/10.1016/j.ccr.2018.03.011.

[91] Grice, K. A., Kubiak, C. P., Chapter five – recent studies of rhenium and manganese bipyridine carbonyl catalysts for the electrochemical reduction of CO_2, Advances in Inorg. Chem. 66 (2014) 163-188. https://doi.org/10.1016/B978-0-12-420221-4.00005-6.

[92] Feng, D.-M., Zhu, Y.-P., Chen, P., Ma, T.-Y., Recent Advances in Transition-Metal-Mediated Electrocatalytic CO_2 Reduction: From Homogeneous to Heterogeneous Systems,

Eclética Química Journal, vol. 44, n. 1, 2019, 11-39
ISSN: 1678-4618
DOI: 10.26850/1678-4618eqj.v44.1.2019.p11-39

Catalysts 7 (12) (2017) 373. https://doi.org/10.3390/catal7120373.

[93] Grice, K. A., Carbon dioxide reduction with homogenous early transition metal complexes: Opportunities and challenges for developing CO_2 catalysis, Coord. Chem. Rev. 336 (2017) 78-95. https://doi.org/10.1016/j.ccr.2017.01.007.

[94] Yamazaki, Y., Takeda, H., Ishitani, O., Photocatalytic reduction of CO_2 using metal complexes C, J. Photochem. Photobiol. 25 (2015) 106-137. https://doi.org/10.1016/j.jphotochemrev.2015.09.001.

[95] Stanbury, M., Compain, J.-D., Chardon-Noblat, S., Electro and photoreduction of CO_2 driven by manganese-carbonyl molecular catalysts, Coord. Chem. Rev. 361 (2018): 120-137. https://doi.org/10.1016/j.ccr.2018.01.014.

[96] Fei, H., Sampson, M. D., Lee, Y., Kubiak, C. P., Cohen, S. M., Photocatalytic CO_2 Reduction to Formate Using a Mn(I) Molecular Catalyst in a Robust Metal–Organic Framework, Inorg. Chem. 54 (14) (2015) 6821-6828. https://doi.org/10.1021/acs.inorgchem.5b00752.

[97] Wang, B., Huang, H., Lv, X.-L., Xie, Y., Li, M.; Li, J.-R., Tuning CO_2 Selective Adsorption over N_2 and CH_4 in UiO-67 Analogues through Ligand Functionalization, Inorg. Chem. 53 (17) (2014) 9254-9259. https://doi.org/10.1021/ic5013473.

[98] Ko, N., Hong, J., Sung, S., Cordova, K. E., Park, H. J., Yang, J. K., Kim, A significant enhancement of water vapour uptake at low pressure by amine-functionalization of UiO-67, J. Dalton Trans. 44 (5) (2015) 2047-2051. https://doi.org/10.1039/C4DT02582B.

[99] Katz, M. J., Brown, Z. J., Colon, Y. J., Siu, P. W., Scheidt, K. A., Snurr, R. Q., Hupp, J. T., Farha, O. K., A facile synthesis of UiO-66, UiO-67 and their derivatives, Chem. Commun. 49 (82) (2013) 9449-9451. https://doi.org/10.1039/c3cc46105j.

[100] Georgopoulos, M., Hoffman, M. Z. J., Cage escape yields in the quenching of tris (2,2'-bipyridine) ruthenium (II) by methylviologen: presence of triethanolamine as a sacrificial electron donor, Phys. Chem. 95 (20) (1991) 7717-7721. https://doi.org/10.1021/j100173a031.

[101] Morimoto, T., Nakajima, T., Sawa, S., Nakanishi, R., Imori, D., Ishitani, O., CO_2 Capture by a Rhenium(I) Complex with the Aid of Triethanolamine, J. Am. Chem. Soc. 135 (45) (2013) 16825-16828. https://doi.org/10.1021/ja409271s.

[102] Hawecker, J., Lehn, J.-M., Ziessel, R., Efficient photochemical reduction of CO_2 to CO by visible light irradiation of systems containing $Re(bipy)(CO)_3X$ or $Ru(bipy)_3^{2+}$–Co^{2+} combinations as homogeneous catalysts, Chem. Soc., Chem. Commun. 0 (9) (1983) 536-538. https://doi.org/10.1039/C39830000536.

[103] Hori, H., Takano, Y., Koike, K., Sasaki, Y., Efficient rhenium-catalyzed photochemical carbon dioxide reduction under high pressure, Inorg. Chem. Commun. 6 (3) (2003) 300-303. https://doi.org/10.1016/S1387-7003(02)00758-X.

[104] Shinozaki, K., Hayashi, Y., Brunschwig, B., Fujita, E., Characterization of transient species and products in photochemical reactions of Re(dmb)$(CO)_3$ Et with and without CO_2, Res. Chem. Intermed. 33 (1-2) (2007) 27-36. https://doi.org/10.1163/156856707779160807.

[105] Fujita, E., Hayashi, Y., Kita, S., Brunschwig, B. S., In Studies in Surface Science and Catalysis; Sang-Eon Park, J.-S. C., Kyu-Wan, L., Eds.; Elsevier: New York, 2004; Vol. 153, p 271.

[106] Agarwal, J., Johnson, R. P., Li, G., A Reduction of CO_2 on a Tricarbonyl Rhenium(I) Complex: Modeling a Catalytic Cycle, J. Phys.

Chem. 115 (13) (2011) 2877-2881. https://doi.org/10.1021/jp111342r.

[107] Hayashi, Y., Kita, S., Brunschwig, B. S., Fujita, E., Involvement of a Binuclear Species with the Re−C(O)O−Re Moiety in CO_2Reduction Catalyzed by Tricarbonyl Rhenium(I) Complexes with Diimine Ligands: Strikingly Slow Formation of the Re−Re and Re−C(O)O−Re Species from Re(dmb)$(CO)_3$S (dmb = 4,4'-Dimethyl-2,2'-bipyridine, S = Solvent), J. Am. Chem. Soc. 125 (39) (2003) 11976-11987. https://doi.org/10.1021/ja035960a.

[108] Franco, F., Pinto, M. F., Royo, B., Lloret-Fillol, J., A Highly Active N-Heterocyclic Carbene Manganese(I) Complex for Selective Electrocatalytic CO_2 Reduction to CO, Angew. Chem. Int. Ed. 57 (17) (2018). https://doi.org/10.1002/anie.201800705.

[109] Bourrez, M., Molton, F., Chardon-Noblat, S., Deronzier, A., [Mn(bipyridyl)$(CO)_3$Br]: An Abundant Metal Carbonyl Complex as Efficient Electrocatalyst for CO_2 Reduction, Angew. Chem. Int. Ed. 123 (2011) 10077-10080. https://doi.org/10.1002/anie.201103616.

[110] Smieja, J. M., Sampson, M. D., Grice, K. A., Benson, E. E., Froehlich, J. D., Kubiak, C. P., Manganese as a substitute for rhenium in CO_2 reduction catalysts: the importance of acids, Inorg. Chem. 52 (5) (2013) 2484-2491. https://doi.org/10.1021/ic302391u.

[111] Sampson, M. D., Nguyen, A. D., Grice, K. A., Moore, C. E., Rheingold, A. L., Kubiak, C. P., Manganese catalysts with bulky bipyridine ligands for the electrocatalytic reduction of carbon dioxide: Eliminating dimerization and altering catalysis, J. Am. Chem. Soc. 136 (14) (2014) 5460-5471. https://doi.org/10.1021/jacs.5b01552.

[112] Franco, F., Cometto, C., Nencini, L., Barolo, C., Sordello, F., Minero, C., Fiedler, J., Robert, M., Gobetto, R., Nervi, C., Local Proton Source in Electrocatalytic CO_2 Reduction with [Mn(bpy–R)$(CO)_3$Br] Complexes, Chem. Eur. J. 23 (20) (2017) 4782. https://doi.org/10.1002/chem.201605546.

[113] Ngo, K. T., McKinnon, M., Mahanti, B., Narayanan, R., Grills, D. C., Ertem, M. Z., J. Rochford J., Turning on the Protonation-First Pathway for Electrocatalytic CO_2 Reduction by Manganese Bipyridyl Tricarbonyl Complexes, J. Am. Chem. Soc. 139 (7) (2017) 2604-2618. https://doi.org/10.1021/jacs.6b08776.

[114] Sampson, M. D., Kubiak, C. P., Manganese Electrocatalysts with Bulky Bipyridine Ligands: Utilizing Lewis Acids To Promote Carbon Dioxide Reduction at Low Overpotentials, J. Am. Chem. Soc. 138 (4) (2016) 1386-1393. https://doi.org/10.1021/jacs.5b12215.

[115] Reuillard, B., Ly, K. H., Rosser, T. E., Kuehnel, M. F., Zebger, I., Reisner, E., Tuning Product Selectivity for Aqueous CO_2 Reduction with a Mn(bipyridine)-pyrene Catalyst Immobilized on a Carbon Nanotube Electrode, J. Am. Chem. Soc. 139 (41) (2017) 14425-14435. https://doi.org/10.1021/jacs.7b06269.

[116] Franco, F., Cometto, C., Vallana, F. F., Sordello, F., Priola, E., Minero, C., Nervi, C., Gobetto, R., A local proton source in a [Mn (bpy-R)$(CO)_3$Br]-type redox catalyst enables CO_2 reduction even in the absence of Brønsted acids, Chem. Commun. 50 (93) (2014) 14670-14673. https://doi.org/10.1039/c4cc05563b.

[117] Smieja, J. M., Sampson, M. D., Grice, K. A., Benson, E. E., Froehlich, J. D., Kubiak, C. P., Manganese as a Substitute for Rhenium in CO_2 Reduction Catalysts: The Importance of Acids, Inorg. Chem. 52 (5) (2013) 2484-2491. https://doi.org/10.1021/ic302391u.

[118] Fei, H., Sampson, M. D., Lee, Y., Kubiak, C. P., Cohen, S. M., Photocatalytic CO_2 Reduction to Formate Using a Mn(I) Molecular Catalyst in a Robust Metal-Organic Framework, Inorg. Chem.

54 (14) (2015) 6821-6828. https://doi.org/10.1021/acs.inorgchem.5b00752.

[119] Agarwal, J., Shaw, T. W., Schaefer, H. F., Bocarsly, A. B., Design of a Catalytic Active Site for Electrochemical CO_2 Reduction with Mn(I)-Tricarbonyl Species, Inorg. Chem. 54 (11) (2015) 5285-5294. https://doi.org/10.1021/acs.inorgchem.5b00233.

[120] Takeda, H., Koizumi, H., Okamoto, K., Ishitani, O., Photocatalytic CO_2 reduction using a Mn complex as a catalyst, Chem. Commun. 50 (12) (2014) 1491-1493. https://doi.org/10.1039/c3cc48122k.

[121] Ngo, K. T., McKinnon, M., Mahanti, B., Narayanan, R., Grills, D. C., Ertem, M. Z., Rochford, Turning on the Protonation-First Pathway for Electrocatalytic CO_2 Reduction by Manganese Bipyridyl Tricarbonyl Complexes, J. J. Am. Chem. Soc. 139 (7) (2017) 2604-2618. https://doi.org/10.1021/jacs.6b08776.

[122] Franco, F., Cometto, C., Nencini, L., Barolo, C., Sordello, F., Minero, C., Fiedler, J., Robert, M., Gobetto, R., Nervi, C., Local Proton Source in Electrocatalytic CO_2 Reduction with [Mn(bpy–R)$(CO)_3$Br] Complexes, Chem. - Eur. J. 23 (20) (2017) 4782-4793. https://doi.org/10.1002/chem.201605546.

[123] Walsh, J. J., Smith, C. L., Neri, G., Whitehead, G. F. S., Robertson, C. M., Cowan, A. J., Improving the efficiency of electrochemical CO_2 reduction using immobilized manganese complexes, Faraday Discuss. 183 (2015) 147-160. https://doi.org/10.1039/c5fd00071h.

[124] Torralba-Peñalver, E.; Luo, Y.; Compain, J.-D.; Chardon-Noblat, S.; Fabre, B., Selective Catalytic Electroreduction of CO_2 at Silicon Nanowires (SiNWs) Photocathodes Using Non-Noble Metal-Based Manganese Carbonyl Bipyridyl Molecular Catalysts in Solution and Grafted onto SiNWs, ACS Catal. 5 (10) (2015) 6138-6147. https://doi.org/10.1021/acscatal.5b01546.

[125] Rosser, T. E., Windle, C. D., Reisner, E., Electrocatalytic and Solar-Driven CO_2 Reduction to CO with a Molecular Manganese Catalyst Immobilized on Mesoporous TiO_2, Angew. Chem., Int. Ed. 55 (26) (2016) 7388. https://doi.org/10.1002/anie.201601038.

[126] Bourrez, M., Orio, M., Molton, F., Vezin, H., Duboc, C., Deronzier, A., Chardon-Noblat, S., Pulsed-EPR Evidence of a Manganese (II) Hydroxycarbonyl Intermediate in the Electrocatalytic Reduction of Carbon Dioxide by a Manganese Bipyridyl Derivative, Angew. Chem., Int. Ed. 53 (1) (2014) 240-243. https://doi.org/10.1002/anie.201306750.

[127] Keim, W., Nickel: an element with wide application in industrial homogeneous catalysis, Angew. Chem. Int. Ed. Engl. 29 (3) (1990) 235-244. https://doi.org/10.1002/anie.199002351.

[128] Rosen, B. M., Quasdorf, K. W., Wilson, D. A., Zhang, N., Resmerita, A.-M., Garg, N. K., Percec, V., Nickel-catalyzed cross-couplings involving carbon-oxygen bonds, Chem. Rev. 111 (3) (2011) 1346-1416. https://doi.org/10.1021/cr100259t.

[129] Wiese, S., Kilgore, U. J., DuBois, D. L., Bullock, R. M., $[Ni(P^{Me}{}_2N^{Ph}{}_2)_2](BF_4)_2$ as an Electrocatalyst for H_2 Production, ACS Catal. 2 (5) (2012) 720-727. https://doi.org/10.1021/cs300019h.

[130] Gan, L., Groy, T. L., Tarakeshwar, P., Mazinani, S. K., Shearer, J., Mujica, V., Jones, A. K., A nickel phosphine complex as a fast and efficient hydrogen production catalyst, J. Am. Chem. Soc. 137 (3) (2015) 1109-1115. https://doi.org/10.1021/ja509779q.

[131] Thoi, V. S., Kornienko, N., Margarit, C. G., Yang, P., Chang, C. J., Visible-Light Photoredox Catalysis: Selective Reduction of Carbon Dioxide

to Carbon Monoxide by a Nickel N-Heterocyclic Carbene–Isoquinoline Complex, J. Am. Chem. Soc. 135 (38) (2013) 14413-14424. https://doi.org/10.1021/ja4074003.

[132] Han, Y., Wu, Y., Lai, W., Cao, R., Electrocatalytic water oxidation by a water-soluble nickel porphyrin complex at neutral pH with low overpotential, Inorg. Chem. 54 (11) (2015) 5604-5613. https://doi.org/10.1021/acs.inorgchem.5b00924.

[133] Zhang, M., Zhang, M. T., Hou, C., Ke, Z. F., Lu, T. B., Homogeneous electrocatalytic water oxidation at neutral pH by a robust macrocyclic nickel (II) complex, Angew. Chem. Int. Ed. 53 (48) (2014) 13042-13048. https://doi.org/10.1002/anie.201406983.

[134] Solis, B. H., Maher, A. G., Dogutan, D. K., Nocera, D. G., Hammes-Schiffer, S., Nickel phlorin intermediate formed by proton-coupled electron transfer in hydrogen evolution mechanism, Proc. Natl. Acad. Sci. U.S.A. 113 (3) (2016) 485-492. https://doi.org/10.1073/pnas.1521834112.

[135] Zilbermann, I., Maimon, E., Cohen, H., Meyerstein, D., Redox chemistry of nickel complexes in aqueous solutions, Chem. Rev. 105 (6) (2005) 2609-2626. https://doi.org/10.1021/cr030717f.

[136] Tasker, S. Z., Standley, E. A., Jamison, T. F., Recent advances in homogeneous nickel catalysis, Nature 509 (2014) 299-309. https://doi.org/10.1038/nature13274.

[137] Beley, M., Collin, J. P., Ruppert, R., Sauvage, J. P., Electrocatalytic reduction of carbon dioxide by nickel cyclam^{2+} in water: study of the factors affecting the efficiency and the selectivity of the process, J. Am. Chem. Soc. 108 (4) (1986) 7461-7467. https://doi.org/10.1021/ja00284a003.

[138] Helm, M. L., Stewart, M. P., Bullock, R. M., DuBois, M. R., DuBois, D. L., A synthetic nickel electrocatalyst with a turnover frequency above 100,000 s^{-1} for H_2 production, Science 333 (2011) 863-866. https://doi.org/10.1126/science.1205864.

[139] Shafaat, H. S., Rudiger, O., Ogata, H., Lubitz, W., [NiFe] hydrogenases: a common active site for hydrogen metabolism under diverse conditions, Biochim. Biophys. Acta 1827 (8-9) (2013) 986-1002. https://doi.org/10.1016/j.bbabio.2013.01.015.

[140] Greene, B. L., Wu, C. H., Vansuch, G. E., Adams, M. W., Dyer, R. B., Proton Inventory and Dynamics in the Ni_a-S to Ni_a-C Transition of a [NiFe] Hydrogenase, Biochemistry 55 (12) (2016) 1813-1825. https://doi.org/10.1021/acs.biochem.5b01348.

[141] Jeoung, J. H., Dobbek, H., Carbon dioxide activation at the Ni, Fe-cluster of anaerobic carbon monoxide dehydrogenase, Science 318 (2007) 1461-1464. https://doi.org/10.1126/science.1148481.

[142] Fesseler, J., Jeoung, J.-H., Dobbek, H., How the $[NiFe_4S_4]$ Cluster of CO Dehydrogenase Activates CO_2 and NCO^-, Angew. Chem. Int. Ed. 54 (29) (2015) 8560-8564. https://doi.org/10.1002/anie.201501778.

[143] Dempsey, J. L., Brunschwig. B. S., Winkler, J. R., Gray, H. B., Hydrogen evolution catalyzed by cobaloximes, Acc. Chem. Res. 42 (12) (2009) 1995-2004. https://doi.org/10.1021/ar900253e.

[144] Wang, M., Na, Y., Gorlov, M., Sun, L., Light-driven hydrogen production catalysed by transition metal complexes in homogeneous systems, Dalton Trans. (2009) 6458-6467. https://doi.org/10.1039/b903809d.

[145] Mondal, B., Dey, A., Development of air-stable hydrogen evolution catalysts, Chem. Commun. 53 (55) (2017) 7707-7715. https://doi.org/10.1039/c7cc02941a.

Eclética Química Journal, vol. 44, n. 1, 2019, 11-39
ISSN: 1678-4618
DOI: 10.26850/1678-4618eqj.v44.1.2019.p11-39

[146] Zee, D. Z., Chantarojsiri, T., Long, J. R., Chang, C. J., Metal-polypyridyl catalysts for electro-and photochemical reduction of water to hydrogen, Acc. Chem. Res. 48 (7) (2015) 2027-2036. https://doi.org/10.1021/acs.accounts.5b00082.

[147] Wang, M., Chen, L., Sun, L., Recent progress in electrochemical hydrogen production with earth-abundant metal complexes as catalysts, Energy Environ. Sci. 5 (5) (2012) 6763-6778. https://doi.org/10.1039/C2EE03309G.

[148] Thoi, V. S., Sun, Y., Long, J. R., Chang, C. J., Complexes of earth-abundant metals for catalytic electrochemical hydrogen generation under aqueous conditions, Chem. Soc. Rev. 42 (6) (2013) 2388-2400. https://doi.org/10.1039/c2cs35272a.

[149] Coutard, N., Kaeffer, N., Artero, V., Molecular engineered nanomaterials for catalytic hydrogen evolution and oxidation, Chem. Commun. 52 (95) (2016) 13728-13748. https://doi.org/10.1039/c6cc06311j.

[150] Willkomm, J., Orchard, K. L., Reynal, A., Pastor, E., Durrant, J. R., Reisner, E., Dye-sensitised semiconductors modified with molecular catalysts for light-driven H_2 production, Chem. Soc. Rev. 45 (1) (2016) 9-23. https://doi.org/10.1039/c5cs00733j.

[151] DuBois, D. L., Bullock, R. M., Molecular electrocatalysts for the oxidation of hydrogen and the production of hydrogen – the role of pendant amines as proton relays, Eur. J. Inorg. Chem. 2011 (7) (2011) 1017-1027. https://doi.org/10.1002/ejic.201001081.

[152] Kärkäs, M. D., Verho, O., Johnston, E. V., Åkermark, B., Artificial photosynthesis: molecular systems for catalytic water oxidation, Chem. Rev. 114 (24) (2014) 11863-12001. https://doi.org/10.1021/cr400572f.

[153] Kondo, M., Masaoka, S., Water oxidation catalysts constructed by biorelevant first-row metal complexes, Chem. Lett. 45 (11) (2016) 1220-1231. https://doi.org/10.1246/cl.160639.

[154] Garrido-Barros, P., Gimbert-Surinach, C., Matheu, R., Sala, X., Llobet, A., How to make an efficient and robust molecular catalyst for water oxidation, Chem. Soc. Rev. 46 (20) (2017) 6088-6098. https://doi.org/10.1039/c7cs00248c.

[155] Costentin, C., Robert, M., Savéant, J.-M., Current Issues in Molecular Catalysis Illustrated by Iron Porphyrins as Catalysts of the CO_2-to-CO Electrochemical Conversion, Acc. Chem. Res. 48 (12) (2015) 2996-3006. https://doi.org/10.1021/acs.accounts.5b00262.

[156] Benson, E. E., Kubiak, C. P., Sathrum, A. J., Smieja, J. M., Electrocatalytic and homogeneous approaches to conversion of CO_2 to liquid fuels, Chem. Soc. Rev. 38 (1) (2009) 89-99. https://doi.org/10.1039/b804323j.

[157] Yamazaki, Y., Takeda, H., Ishitani, O., Photocatalytic reduction of CO_2 using metal complexes C, J. Photochem. Photobiol. 25 (2015) 106-137. https://doi.org/10.1016/j.jphotochemrev.2015.09.001.

[158] Morris, A. J., Meyer, G. J., Fujita, E., Molecular approaches to the photocatalytic reduction of carbon dioxide for solar fuels, Acc. Chem. Res. 42 (12) (2009) 1983-1994. https://doi.org/10.1021/ar9001679.

[159] Reithmeier, R., Bruckmeier, C., Rieger, B., Conversion of CO_2 via visible light promoted homogeneous redox catalysis, Catalysts 2 (4) (2012) 544-571. https://doi.org/10.3390/catal2040544.

[160] Kang, P., Chen, Z., Brookhart, M., Meyer, T. J., Electrocatalytic reduction of carbon dioxide: Let the molecules do the work, Top. Catal. 58 (1)

Eclética Química Journal, vol. 44, n. 1, 2019, 11-39
ISSN: 1678-4618
DOI: 10.26850/1678-4618eqj.v44.1.2019.p11-39

(2014) 30-45. https://doi.org/10.1007/s11244-014-0344-y.

[161] Windle, C. D., Perutz, R. N., Advances in molecular photocatalytic and electrocatalytic CO_2 reduction, Coord. Chem. Rev. 256 (2012) 2562-2570. https://doi.org/10.1016/j.ccr.2012.03.010.

[162] Costentin, C., Robert, M., Savéant, J.-M., Catalysis of the electrochemical reduction of carbon dioxide, Chem. Soc. Rev. 42 (6) (2013) 2423-2436. https://doi.org/10.1039/c2cs35360a.

[163] Wang, J.-W., Zhong, D.-C., Lu, T.-B., Artificial photosynthesis: Catalytic water oxidation and CO_2 reduction by dinuclear non-noble-metal molecular catalysts, Coord. Chem. Rev. 377 (2017) 225-236. https://doi.org/10.1016/j.ccr.2018.09.003.

[164] Niu, K., Xu, Y., Wang, H., Ye, R., Xin, H. L., Lin, F., Tian, C., Lum, Y., Bustillo, K. C., Doeff, M. M., Koper, M. T. M., Ager, J., Xu, R., Zheng, H., A spongy nickel-organic CO_2 reduction photocatalyst for nearly 100% selective CO production, Sci. Adv. 3 (7) (2017) 1-9. https://doi.org/10.1126/sciadv.1700921.

[165] Gao, C., Meng, Q., Zhao, K., Yin, H., Wang, D., Guo, J., Zhao, S., Chang, L., He, M., Li, Q., Zhao, H., Huang, X., Gao, Y., Tang, Z., Co_3O_4 Hexagonal Platelets with Controllable Facets Enabling Highly Efficient Visible-Light Photocatalytic Reduction of CO_2, Adv. Mater. 28 (30) (2016) 6485-6490. https://doi.org/10.1002/adma.201601387.

[166] Kirch, M., Lehn, J.-M., Sauvage, J.-P., Hydrogen generation by visible light irradiation of aqueous solutions of metal complexes. An approach to the photochemical conversion and storage of solar energy, Helv. Chim. Acta 62 (4) (1979) 1345-1384. https://doi.org/10.1002/hlca.19790620449.

[167] Gärtner, F., Sundararaju, B., Surkus, A.-E., Boddien, A., Loges, B., Junge, H., Dixneuf, P. H., Beller, M., Light-Driven Hydrogen Generation: Efficient Iron-Based Water Reduction Catalysts, Angew. Chem. Int. Ed. 48 (52) (2009) 9962-9965. https://doi.org/10.1002/anie.200905115.

[168] Maschmeyer, T., Che, M., Catalytic Aspects of Light-Induced Hydrogen Generation in Water with TiO_2 and Other Photocatalysts: A Simple and Practical Way Towards a Normalization?, Angew. Chem. Int. Ed. 49 (9) (2010) 1536-1539. https://doi.org/10.1002/anie.200903921.

[169] Cheng, T., Xiao, H., Goddard III, W. A., Full atomistic reaction mechanism with kinetics for CO reduction on Cu (100) from ab initio molecular dynamics free-energy calculations at 298 K, Proc. Natl. Acad. Sci. U.S.A. 114 (8) (2017) 1795-1800. https://doi.org/10.1073/pnas.1612106114.

[170] Li, C. W., Ciston, J., Kanan, M. W., Electroreduction of carbon monoxide to liquid fuel on oxide-derived nanocrystalline copper, Nature 508 (2014) 504-507. https://doi.org/10.1038/nature13249.

[171] London, R. E., Walker, T. E., Kollman, V. H., Matwiyoff, N. A., Studies of the pH dependence of carbon-13 shifts and carbon-carbon coupling constants of [U-13C] aspartic and-glutamic acids, J. Am. Chem. Soc. 100 (12) (1978) 3723-3729. https://doi.org/10.1021/ja00480a012.

[172] Kuehnel, M. F., Orchard, K. L., Dalle, K. E., Reisner, E., Selective Photocatalytic CO_2 Reduction in Water through Anchoring of a Molecular Ni Catalyst on CdS Nanocrystals, J. Am. Chem. Soc. 139 (21) (2017) 7217-7223. https://doi.org/10.1021/jacs.7b00369.

ISSN: 1678-4618
DOI: 10.26850/1678-4618eqj.v44.1.2019.p11-39